Molecular Mechanisms of Apoptotic Resistance

Honors Research Thesis

Presented in Partial Fulfillment of the Requirements for graduation
with Honors Research Distinction in the undergraduate colleges of
The Ohio State University

by

Justin C. Tossey

The Ohio State University
May 2013

Project Advisor: Dr. Andrea I. Doseff, Associate Professor,
Department of Molecular Genetics, Department of Internal Medicine

Dedication

This document is dedicated to my parents, for their love and unyielding support.

Table of Contents

Abbreviations

7-AAD	7-Amino-actinomycin D
A or Ala	Alanine
aa	Amino acid
AC	Adenocarcinoma
AFC	7-amino-4-trifluoromethylcoumarin
Akt	Protein kinase B
APAF-1	Apoptotic protease-activating factor-1
APC	Allophycocyanin
ATCC	American Type Culture Collection
ATP	Adenosine-triphosphate
Bak	Bcl-2 homologous antagonist/killer
Bax	Bcl-2-associated X protein
Bcl-2	B-cell lymphoma 2
Bcl-X_L	B-cell lymphoma-extra large
BID	BH3 interacting-domain death agonist
BIR	Baculovirus IAP repeat
BSA	Bovine serum albumin
C or Cys	Cysteine
c-FLIP	Cellular FLICE inhibitory protein
CI	Combination index
D or Asp	Aspartic acid
DcR1 and 2	Decoy receptor 1 and 2

DISC	Death inducing signaling complex
DMEM	Dulbecco's modified eagle medium
DMSO	Dimethyl sulfoxide
dNTP	Deoxyribonucleotide
Dox	Doxorubicin
DR5	Death receptor 5
DTT	Dithiothreitol
E or Glu	Glutamic acid
EDTA	Ethylenediaminetetraacetic acid
EGTA	Ethylene glycol tetraacetic acid
FADD	Fas-associated death domain
FBS	Fetal bovine serum
FITC	Fluorescein isothiocyanate
FL	Full-length
FLICE	FADD-like interleukin-1 β-converting enzyme (caspase-8)
H or His	Histidine
HEPES	Hydroxyethyl piperazineethanesulfonic acid
HRP	Horseradish peroxidase
Hsp	Heat shock protein
I or Ile	Isoleucine
IAP	Inhibitor of apoptosis
Ig	Immunoglobulin
IP	Immunoprecipitation

IPTG	Isopropyl β-D-1-thiogalactopyranoside
L or Leu	Leucine
LB	Lysogeny broth
LCC	Large cell carcinoma
MK2	Mitogen-activated protein kinase-activated protein kinase 2
MTS	3-(4,5-dimethylthiazol-2-yl)-5-(3-carboxymethoxyphenyl)-2-(4-sulfophenyl)-2H-tetrazolium
NP-40	Nonidet P-40
NSCLC	Non-small cell lung carcinoma
Ni^{2+}-NTA	Nickel-nitrilotriacetic acid
PAGE	Polyacrylamide gel electrophoresis
PBS	Phosphate buffered saline
PCR	Polymerase chain reaction
PDB	Protein data bank
PE	Phycoerythrin
PIPES	1,4-piperazinediethanesulfonic acid
PKC	Protein kinase C
PMSF	Phenylmethanesulfonylfluoride
P/S	Penicillin/streptomycin
ROS	Reactive oxygen species
RPMI	Rosewell Park Memorial Institute medium
S or Ser	Serine
SCC	Small cell carcinoma

SCLC	Small cell lung carcinoma
SDS	Sodium dodecylsulfate
SmN	Survival of motor neuron protein
SOC	Super optimal broth
T or Thr	Threonine
TAE	Tris-acetate EDTA
TBS-T	Tris-buffered saline-Tween-20
TNF	Tumor necrosis factor
TRAIL	TNF-related apoptosis-inducing ligand
UV	Ultraviolet
V or Val	Valine
wt	Wild-type
XIAP	X-linked inhibitor of apoptosis

Chapter 1

Introduction

1.1 Cancer

Cancer, broadly defined as abnormal cells that grow and divide uncontrollably, is the second leading cause of death in the U.S. with more than 500,000 deaths in 2009 (1). In general, cancers are caused by a series of genetic abnormalities including mutations of tumor suppressors, like p53, transcriptional or translational mechanisms that cause the overexpression of survival proteins, like heat shock protein 27 (Hsp27), and splicing mechanisms that can alternate the ratios of pro- and anti-apoptotic proteins, such as the cellular FLICE-inhibitory protein (c-FLIP long vs. short) (2-5). These mutations result in transformed cells with prolonged lifespan, which resist the normal signals that induce programmed cell death, or apoptosis. Treatments vary depending on the type of cancer and how early it is detected, but could include surgery, chemotherapy, radiation therapy, and palliative care (6).

Lung cancer has both the highest rate of incidence as well as the greatest mortality rate of any cancer in the U.S. with 200,000 new cases and a 75% mortality rate in 2010 (7). Lung cancers are divided histologically into small cell lung carcinomas (SCLC) and non-small cell lung carcinomas (NSCLC). NSCLC account for 85% of all lung cancer cases and are further subdivided into adenocarcinomas (AC, 40%), squamous cell carcinomas (SCC, 40%), and large cell carcinomas (LCC, 20%) (8,9). Approximately 70% of all NSCLCs are diagnosed in the advanced stage in which the cancer has already begun to metastasize from the lung to other organs of the body, including local lymph nodes and the brain (8). Once

NSCLCs have progressed to the advanced stage, the five-year survival rate is less than 1% with limited treatment options, including combination chemotherapy and palliative radiation therapy (10). Cancer cells killed by combination chemotherapies involving platinum agents like cisplatin (DNA damage), mitotic inhibitors including paclitaxel, vinorelbine, and docetaxel (cell cycle arrest), nucleoside analogs such as gemcitabine (DNA damage), and folate anti-metabolites like pemetrexed (disruption of DNA synthesis) have only been shown to extend survival by two months while greatly decreasing the quality of life due to the toxic side effects of multiple chemotherapeutic agents (11). As a result of the high mortality rate and ineffectiveness of treatments, there has been recent interest in identifying novel therapies for the treatment of NSCLCs.

1.2 Apoptosis and Apoptotic Regulators

Apoptosis is the evolutionarily conserved mechanism of cell death essential for normal organismal development and cellular homeostasis (12). This tightly controlled biological process involves numerous proteins and pathways, but it is primarily regulated by a family of conserved cysteine proteases known as the caspases. The first caspase to be identified was ced-3 and was discovered in *C. elegans* (13). Since that time, 13 caspases have been identified in mammals, 12 of which can be found in humans (caspase-11 being the exception). Caspases play a variety of roles, not limited to apoptosis, by contributing to normal development and inflammation. Within apoptosis, caspase-8 and -9 are known as initiator caspases, which transmit the apoptotic signal to caspase-3, -6, and -7, the executioner caspases, which receive the signal and are responsible for the biochemical and physiological changes that occur in an apoptotic cell including DNA fragmentation,

cytoplasmic shrinkage, and membrane blebbing (12,14). All caspases are synthesized as inactive zymogens (or procaspases) and require proteolytic maturation to exhibit enzymatic activity.

Apoptotic signaling occurs via the intrinsic and extrinsic pathways. The extrinsic pathway involves the binding of a ligand to a death receptor. The most studied ligands include Fas and tumor necrosis factor (TNF) family members TNFα and TNF-related apoptosis inducing ligand (TRAIL), which bind to the receptors CD95, TNF-R1 and -R2, and death receptors, DR4 and -5 (15-18). The ligand binding results in the recruitment of the Fas-associated death domain (FADD) protein and procaspase-8 within the cell, which forms the death inducing signaling complex (DISC) leading to activation of caspase-8 (Fig. 14) (17,19). The intrinsic pathway is initiated by cellular stress, such as DNA damage or reactive oxygen species (ROS), often caused by a chemotherapeutic drug or UV irradiation. The stimulus promotes mitochondrial membrane depolarization and the release of cytochrome C, which forms a complex with apoptotic protease activating factor 1 (APAF-1) and procaspase-9 called the apoptosome (20). The association of procaspase-9 with the apoptosome promotes the activation of caspase-9, which in turn initiates the activation of caspase-3 (Fig. 14) (21-23).

Caspase-3 is composed of three domains, an amino-terminal (N-terminal) domain, also known as the prodomain, consisting of 28 amino acids (aa), a middle domain of 17 kDa (p17), and a carboxy-terminal (C-terminal) 12 kDa domain (p12). Activation begins with the enzymatic cleavage of the p12 domain by caspase-8 or -9 at Asp175, followed by the autocatalytic cleavage of the prodomain. Two p17 and two p12 subunits reorganize into a heterodimer to form the active enzyme (Fig. 14) (12,19,21). The active site is formed by

four loops (L1-L4) with L1 and most of L2 found in the p17 domain and the remaining loops being contributed by the p12 domain (24). The p17 domain also contains the active cysteine residue (Cys163) within the L2 loop, which can render caspase-3 inactive when mutated (24). The active heterodimer of caspase-3 then cleaves numerous target proteins that result in the biochemical and physiological changes associated with apoptosis.

Although the extrinsic and intrinsic pathways function independently, a potential crosstalk mechanism between the two signaling pathways that leads to caspase-3 activation has been reported (25). In particular, caspase-8 has been shown to proteolytically process the BH3 interacting-domain death agonist (BID), a B-cell lymphoma 2 (Bcl-2) protein family member, resulting in the accumulation of cleaved *t*-Bid, which re-localizes to the mitochondria to bind to Bcl-2-associated X protein (Bax) or Bcl-2 homologous antagonist/killer (Bak) and cause depolarization of the mitochondrial membrane (Fig. 14) (25,26). Regardless if the extrinsic and/or intrinsic pathways are involved, they both converge at the level of effector caspase activation, making caspase-3 pivotal to the execution of apoptosis.

Excessive apoptosis is believed to be the cause of several autoimmune and neurodegenerative disorders, such as arthritis or Alzheimer's. Conversely, diseases like cancer are characterized by insufficient apoptosis. Therefore, multiple checkpoints tightly regulate this process to ensure the proper execution of apoptosis. In particular, a repertoire of anti-apoptotic proteins, including members of the Bcl-2 family, the inhibitors of apoptosis (IAPs), and the heat shock protein (Hsps) have emerged as important regulators within the apoptotic pathway.

So far, 15 Bcl-2 proteins have been identified in mammalian cells, the best studied being the anti-apoptotic Bcl-2 and B-cell lymphoma-extra large (Bcl-X_L), and the pro-apoptotic Bax and Bak (27). Bcl-2 and Bcl-X_L maintain the integrity of the mitochondrial membrane by binding to the pro-apoptotic Bax and Bak molecules, thereby providing a mechanism by which cell death or survival signals are determined by the ratio of pro- and anti-apoptotic Bcl-2 proteins (28,29). Apoptotic stimuli cause a shift in the ratio between the pro- and anti-apoptotic Bcl-2 family proteins, allowing for the oligomerization of Bax and Bak and the formation of mitochondrial pores which result in the release of cytochrome C and the activation of caspase-3 via caspase-9 (29,30).

The IAP family consists of 8 evolutionarily conserved members originally described in baculovirus, including c-IAP1, c-IAP2, and the X-linked inhibitor of apoptosis (XIAP), which contain at least one Baculovirus IAP Repeat (BIR) domain and function at multiple levels in the apoptotic cascade to prevent cell death (31,32). For instance, c-IAP1 and c-IAP2 proteins inhibit apoptosis by indirectly suppressing caspase-8 activation (31,33). XIAP is able to regulate apoptosis by binding to both caspase-9 and caspase-3 to prevent their activation (Fig. 14) (31,34). In addition, XIAP levels have been found to be elevated in numerous cancers and have recently gained interest as prognostic markers in bladder, colon, and renal cancers (35-38).

Another important group of anti-apoptotic regulators is the Hsp family. Hsps are a large family of conserved chaperones whose expression is increased by cellular stress (e.g. heat and cellular toxins) to prevent protein aggregation and aid in refolding (39). Family members are classified based on their molecular weight and are divided into high- and low-molecular weight proteins. The high-molecular weight Hsps, including Hsp60 and Hsp70,

require ATP to mediate protein folding, while the small Hsps, like Hsp22 and Hsp27, interact with proteins in an ATP-independent manner (39,40). Small Hsps (sHsps) share several structural features including a hydrophobic N-terminal that mediates chaperone activity and contributes to oligomerization, and a hydrophilic C-terminal that contains a highly conserved α-crystallin domain involved in protein-protein interactions (40,41). Monomers of sHsps form homodimers in an anti-parallel orientation that then become the building blocks of structurally diverse functional oligomers ranging from 50 to 800 kDa (40,42). Hsp27, a 27 kDa protein of 205 aa, has emerged as an important anti-apoptotic regulator by interfering with the apoptotic cascade at multiple levels. The Hsp27 protein harbors three phosphorylation sites at Ser15, Ser78, and Ser82 that have been shown to regulate its anti-apoptotic activity by preventing its association with pro-apoptotic molecules when all three sites are phosphorylated (43). The phosphorylation of Hsp27 is mediated by several kinase signaling networks, including the Protein kinase Cδ (PKCδ) and the MK2/p38 pathway (44,45). The N-terminal (specifically aa 51-88) of Hsp27 has been shown to bind to cytochrome C, thereby preventing caspase-9 activation (46). In addition, Hsp27 associates directly to the prodomain of caspase-3 inhibiting the autocatalytic cleavage necessary for its activation (Fig. 14) (21). However, the specific binding domain of Hsp27 responsible for the interaction with caspase-3 has not been elucidated.

1.3 Flavonoids

Flavonoids are plant phytochemicals that are considered non-essential nutrients that provide numerous health benefits. Compounds with bioactive functions that provide health advantages are known as nutraceuticals. Nutraceuticals include soluble fibers, plant

sterols, isothiocyanates, phytoestrogens (e.g. lycopene, resveratrol), and flavonoids (47). There are more than 5,000 flavonoids that can be further subdivided based on structural differences from the core 2-phenyl-4H-chromen-4-one (Flavone; Fig. 1A) structure into flavones, isoflavones, flavonols, flavanols, flavonones, and anthocyanins (47,48).

The health benefits of dietary flavonoids have been extensively documented through numerous studies which show they possess anti-inflammatory, anti-oxidant, and anti-tumorigenic properties (48). Research has shown that flavonoids can reduce the risk of Parkinson's, strokes, and cardiovascular diseases (49-51). The incidence of various cancers, including breast, ovarian, colorectal, and lung, have been shown to be inversely related to the dietary uptake of flavonoids (52-55). These studies demonstrate why flavonoids have attracted attention for their potential therapeutic capabilities. However, epidemiological studies are scarce and the effectiveness of these compounds has yet to be fully determined.

The flavone apigenin (5,7,4'-trihydroxyflavone; Fig. 1B) can be found in a variety of vegetables, fruits, and chamomile tea, but is most abundant in parsley and celery (56-58). Apigenin has anti-carcinogenic, anti-proliferative, and anti-inflammatory properties (59). The bioactivity of apigenin stems from its ability to inhibit proteins like Bcl-2, activate pro-apoptotic proteins like PKCδ, and induce DNA damage, which subsequently leads to apoptosis (60-62). We recently showed that apigenin induces apoptosis in leukemia cells (61). Apigenin has also been shown to cause apoptosis in some solid tumors, such as prostate cancers and breast cancers that express the HER2/*neu* receptor (63,64). However, generally apigenin has been found to simply inhibit mobility, tumor invasion, and tumor growth, as opposed to inducing cell death, especially in lung cancers (65-68). It has

been further demonstrated that apigenin can regulate other cellular pathways by suppressing the cell cycle and inhibiting the function of matrix metalloproteases, fatty acid synthase, and telomerase (69-72). The ability of apigenin to interact with numerous cell systems coupled with its low toxicity to normal cells has made it a promising agent in therapeutic studies. However, the apoptosis-inducing mechanisms by which apigenin functions remain widely unknown and highlight the necessity for a deeper understanding to fully realize its therapeutic potential.

The goals of this thesis were to study mechanisms of apoptosis and the ways in which intracellular proteins and extracellular compounds augment this process. In Chapter 3, we defined the specific region of Hsp27 that is essential for its association with caspase-3 and inhibition of apoptosis. We used clones of Hsp27 with amino acid deletions and discovered two small peptide regions of Hsp27 that are responsible for the interaction with caspase-3. In Chapter 4, we evaluated the ability of apigenin to sensitize NSCLC cells to TRAIL-induced apoptosis. We performed apigenin and TRAIL combination treatments on NSCLC cells and determined that apigenin sensitizes the cells to caspase-3-dependent apoptosis via the downregulation of several anti-apoptotic proteins and disruption of the interaction between DR5 and Hsp70. This research presents a model that contributes to the known complexity of apoptosis as well as supports the possibility of apigenin and TRAIL as novel cancer therapies in the future.

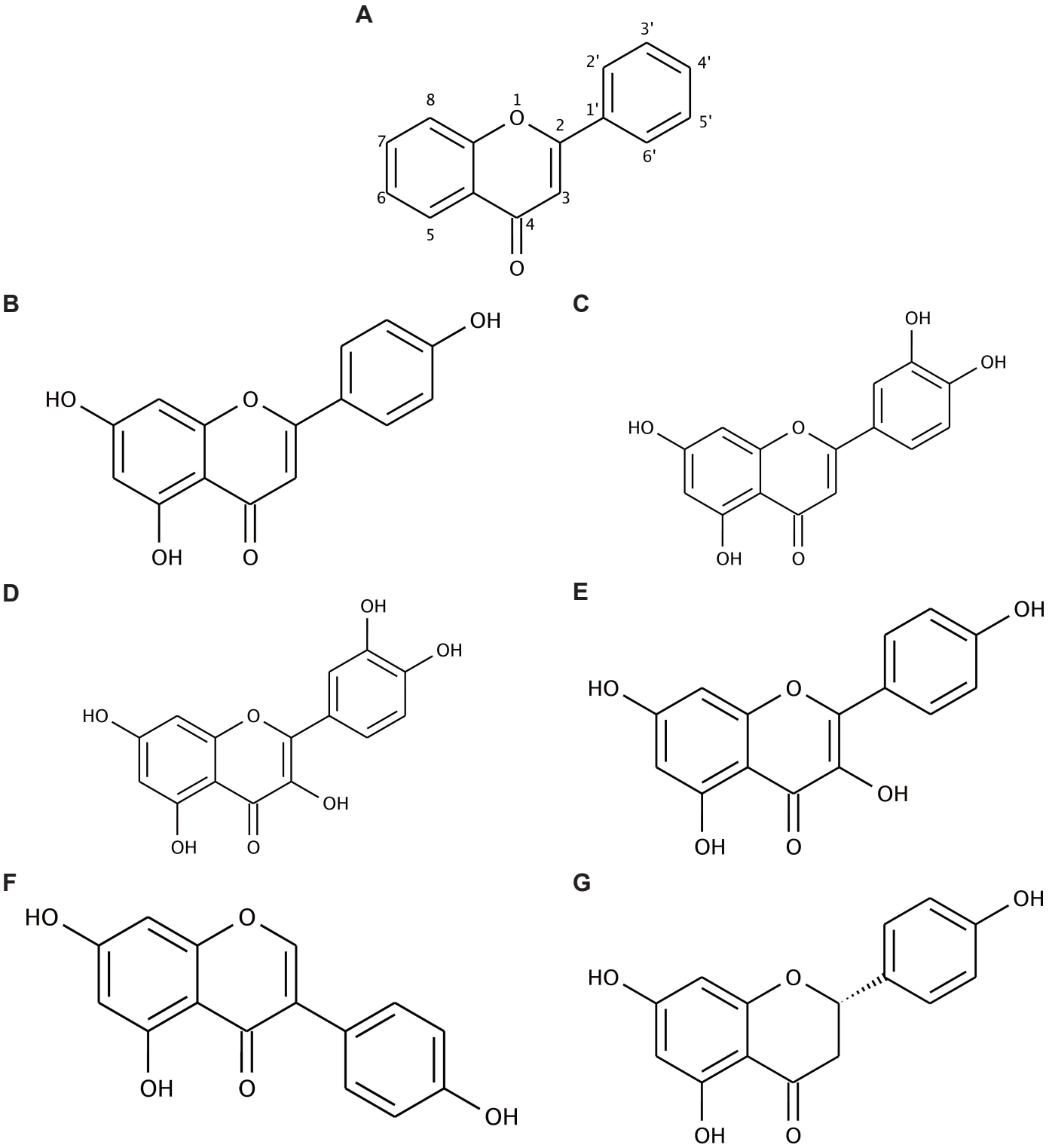

Figure 1. The structures of common flavonoids. **A:** The core flavonoid structure, called "flavone," showing the numbering system for the core flavonoid structure. **B:** The flavone apigenin. **C:** The flavone luteolin. **D:** The flavonol quercetin. **E:** The flavonol kaempferol. **F:** The isoflavone genistein. **G:** The isoflavone naringenin.

Chapter 2

Materials and Methods

2.1 Generation of Clones

2.1.1 Clones into pENTR/D-TOPO Vector

Full-length caspase-3 (AB 249, Table 1) and Hsp27 (AB 262, Table 1) were used as template DNA in PCR reactions to generate caspase-3 wt FL (AB 441, PAO 369/355), Hsp27 wt FL (AB 374, PAO 356/357), Hsp27 N-terminal (AB 827, PAO 356/565), Hsp27 C-terminal (AB 771, PAO 564/357), Hsp27 Δ187-205 (AB 814, PAO 356/559), Hsp27 Δ154-205 (AB 824, PAO 356/560), Hsp27 Δ137-205 (AB 810, PAO 356/561), Hsp27 Δ120-205 (AB 811, PAO 356/562), and Hsp27 Δ104-205 (AB 812, PAO 356/563) into the pENTR/D-TOPO vector (Invitrogen, Carlsbad, CA). Sequences were amplified by PCR to generate clones containing the restriction enzyme sites *BamH*I and *Sal*I or *BamH*I and *Xho*I (Table 1). All PCR reactions were done with 30 ng of template DNA, 12.5 pmol each of forward and reverse primers (Table 2), 50 µM dNTP, 1 x High Fidelity PCR Buffer (Invitrogen), 3 mM $MgCl_2$, and 1 unit High Fidelity Taq Polymerase (1 unit = incorporate 10 nmol of dNTP into DNA in 30 min at 74°C, Invitrogen) in a final volume of 50 µl. The PCR reactions were carried out with 30 cycles under the following conditions: 1 min at 95°C, 1 min at 55°C, and 1 min at 75°C. Products of the PCR reactions were used in ligation reactions to obtain the PCR fragment in the pENTR/D-TOPO vector. For this purpose, 10 ng of PCR product was mixed with 10 ng of pENTR/D-TOPO vector, and 0.25 µl salt solution (6 mM NaCl, 0.3 mM $MgCl_2$) at room temperature for 30 min in a final volume of 5 µl. Ligation reactions were then used to transform *E. coli* Top-10 cells as described in section 2.2 and then plated on

LB-agar (1% (w/v) tryptone, 0.5% (w/v) yeast extract, 0.5% (w/v) NaCl) with 30 μg/ml kanamycin.

2.1.2 Generation of Hsp27 Clones for Mammalian Expression

Hsp27 mutants were cloned into the pCDNA3-5 x myc mammalian expression vector. TOPO-Hsp27 plasmids were digested with *BamH*I and *Xho*I for 3 h at 37°C, run on a 1% agarose gel, and the DNA insert was excised and purified from the gel using the PureLink Quick Gel Extraction Kit following the manufacturer's instructions (Invitrogen). The obtained DNA fragment and pCDNA3-5 x myc vector were ligated at a 10:1 molar ratio with 400 units of T4-ligase (New England Biolabs, Ipswich, MA) in 1 x T4-ligation buffer (50 mM Tris-HCl, 10 mM $MgCl_2$, 10 mM DTT, 1 mM ATP, pH 7.5; New England Biolabs, Ipswich, MA) and distilled water in a total volume of 5 μl. The ligation was incubated at 16°C for 14 h and then the entire reaction was used to transform *E. coli* DH5α cells (Invitrogen) and plated on LB-agar plates with 100 μg/ml ampicillin. Clones were screened for the presence of the correct insert by digesting with *BamH*I and *Xho*I for 3 h at 37°C and running on a 1% agarose gel as described in section 2.2.

2.1.3 Generation of Clones for Bacterial Expression

Caspase-3 and Hsp27 were digested from the pENTR/D-TOPO vector (AB 249 and AB 262, respectively, Table 1) using *BamH*I and *Sal*I enzymes and purified as described above. The obtained DNA fragment and pQE31 or pQE32 vector (for caspase-3 or Hsp27, respectively; Qiagen, Valencia, CA) were ligated at a 10:1 molar ratio with 400 units of T4-ligase in 1 x ligation buffer and distilled water to a total volume of 5 μl for 1 h at room

temperature. Ligation products were used to transform *E. coli* DH5α cells and plated on LB-ampicillin plates and clones were screened by restriction digestion analysis with *BamH*I and *Sal*I enzymes as described in section 2.2.

Table 1. List of Clones

AB Number	Description	Vector	Primers	Restriciton Enzymes	Bacterial Host
AB 249	Caspase-3 wt FL	pENTR/D-TOPO	-	*BamHI/SalI*	DH5α
AB 441	Caspase-3 wt FL	pQE31	PAO 369/355	*BamH*I/*Sal*I	DH5α
AB 262	Hsp27 wt FL	pENTR/D-TOPO	-	*BamHI/SalI*	DH5α
AB 379	Hsp27 wt FL	pCDNA3-5x myc	PAO 356/357	*BamH*I/*Xho*I	DH5α
AB 381	Hsp27 N-terminal	pCDNA3-5x myc	PAO 356/565	*BamH*I/*Xho*I	DH5α
AB 380	Hsp27 C-terminal	pCDNA3-5x myc	PAO 564/357	*BamH*I/*Xho*I	DH5α
AB 374	Hsp27 wt FL	pQE32	PAO 356/357	*BamH*I/*Sal*I	DH5α
AB 827	Hsp27 N-terminal	pQE32	PAO 356/565	*BamH*I/*Sal*I	DH5α
AB 771	Hsp27 C-terminal	pQE32	PAO 564/357	*BamH*I/*Sal*I	DH5α
AB 814	Hsp27 Δ187-205	pENTR/D-TOPO	PAO 356/559	*BamH*I/*Xho*I	Top-10
AB 823	Hsp27 Δ187-205	pCDNA3-5x myc	PAO 356/559	*BamH*I/*Xho*I	DH5α
AB 824	Hsp27 Δ154-205	pENTR/D-TOPO	PAO 356/560	*BamH*I/*Xho*I	Top-10
AB 815	Hsp27 Δ154-205	pCDNA3-5x myc	PAO 356/560	*BamH*I/*Xho*I	DH5α
AB 810	Hsp27 Δ137-205	pENTR/D-TOPO	PAO 356/561	*BamH*I/*Xho*I	Top-10
AB 816	Hsp27 Δ137-205	pCDNA3-5x myc	PAO 356/561	*BamH*I/*Xho*I	DH5α
AB 811	Hsp27 Δ120-205	pENTR/D-TOPO	PAO 356/562	*BamH*I/*Xho*I	Top-10
AB 817	Hsp27 Δ120-205	pCDNA3-5x myc	PAO 356/562	*BamH*I/*Xho*I	DH5α
AB 812	Hsp27 Δ104-205	pENTR/D-TOPO	PAO 356/563	*BamH*I/*Xho*I	Top-10
AB 818	Hsp27 Δ104-205	pCDNA3-5x myc	PAO 356/563	*BamH*I/*Xho*I	DH5α

Table 2. List of Primers

Primer Number	Sequence	Purpose
PAO 355	3'-GAATTCGTCGACTTAGTGATAAAAATAGAG-3'	RP for caspase-3 FL into pQE31
PAO 356	5'-CACCGGGATCCAAGAATTCATGACCGAGCGCCGC-3'	FP for Hsp27 into pCDNA3-5x myc or pQE32
PAO 357	5'-GCTCGAGGTCGACCCCTTGGCGGCAGTCTCATC-3'	RP for Hsp27 into pCDNA3-5x myc or pQE32
PAO 369	5'-CACCGGATCCCCATGGAGAACACTGAAAACTC-3'	FP for caspase-3 FL into pQE31
PAO 559	5'-GCTCGAGGTCGACCCCTCGAAGGTGACTGGGAT-3'	RP for Hsp27 Δ187-205 into pCDNA3-5x myc
PAO 560	5'-GCTCGAGGTCGACCCAACTTGGGTGGGGTCCAC-3'	RP for Hsp27 Δ154-205 into pCDNA3-5x myc
PAO 561	5'-GCTGGAGGTCGACCCCCGGGAGATGTAGCCATG-3'	RP for Hsp27 Δ137-205 into pCDNA3-5x myc
PAO 562	5'-CACCGGGATCCAAGAATTCACCATCCCAGTCACCTTCGAGTC-3'	RP for Hsp27 Δ120-205 into pCDNA3-5x myc
PAO 563	5'-GCTCGAGGTCGACCCGTGGTTGACATCCAGGGA-3'	RP for Hsp27 Δ104-205 into pCDNA3-5x myc
PAO 564	5'-GCTCGAGGTCGACCCCGAGACCCCGCTGCTGAG-3'	FP for Hsp27 C-terminal into pCDNA3-5x myc and pQE32
PAO 565	5'-CACCGGGATCCAAGAATTCGAGATCCGGCACACTGCG-3'	RP for Hsp27 N-terminal into pCDNA3-5x myc and pQE32

FP = forward primer, RP = reverse primer

2.2 Transformation of *E. coli*, Bacterial Culture, and DNA Purification

PCR and ligation products were used to transform either *E. coli* DH5α or Top-10 bacterial cells (Invitrogen; efficiency > 1 x 10^6 cfu/µg DNA and > 1 x 10^9 cfu/µg DNA, respectively). Briefly, 25 µl of cells were incubated with 1 µl of PCR products or 5 µl of ligation products for 30 min on ice. Cells were then subjected to heat shock at 42°C for 45 sec followed by incubation on ice for 2 min. Samples were then given 250 µl of SOC media (2% (w/v) tryptone, 0.5% (w/v) yeast extract, 8.6 mM NaCl, 2.5 mM KCl, 20 mM $MgSO_4$, 20 mM glucose) and incubated at 37°C for 1 h. Finally, cells were plated on LB-agar plates with the appropriate selective antibiotic and allowed to grow overnight at 37°C.

For bacterial liquid culture, one bacterial colony was inoculated into a 14 ml culture tube containing 3 ml of LB broth (1% (w/v) tryptone, 0.5% (w/v) yeast extract, 0.5% (w/v) NaCl) with appropriate antibiotics and the culture was grown at 37°C for 16 h. Plasmid DNA was purified using the QIAprep Miniprep Spin Kit following the manufacturer's instructions (Qiagen). The purified plasmid DNA was digested to screen for positive clones using 0.5 µg of DNA in a 10 µl reaction with 1 x BSA, 1 x appropriate NEBuffer (Buffer 3: 100 mM NaCl, 50 mM Tris-HCl, 10 mM $MgCl_2$, 1 mM DTT, pH 7.9; New England Biolabs), 5,000 units of each restriction enzyme (Table 1), and distilled water. The digestion was performed at 37°C for 3 h. DNA loading buffer 6 x (0.25% bromophenol blue and 30% glycerol in water) was added to the digestion product to reach 1 x and samples were run on a 1% agarose gel containing 0.2 µg/ml ethidium bromide in TAE Buffer (40 mM Tris-acetate, 1 mM EDTA, pH 8.0) using the 1 Kb plus DNA ladder (Invitrogen) to verify the size of the digested fragments. The gel was run for 30 min at 100 V and DNA fragments were cut and purified using the PureLink Quick Gel Extraction Kit as described in section 2.1.2.

2.3 Cell Tissue Culture

HeLa (human cervical cancer), H9c2 (rat cardiomyocyte), A549 (Stage I lung ACC), H2009 (Stage IV lung ACC), and H1299 (lung LCC) cells obtained from the American Type Culture Collection (ATCC) and Calu-1 (Stage III lung SCC) cells generously donated by Dr. Croce (Ohio State University), were grown at 37°C in an atmosphere of 5% CO_2. HeLa, H9c2, A549, H2009, and H1299 cells were cultured in high glucose Dulbecco's modified Eagle's medium (DMEM; Life Technologies, Grand Island, NY) supplemented with 5% fetal bovine serum (FBS) and 1% penicillin and streptomycin solution (P/S; BioWhittaker, Walkersville, MD), while Calu-1 cells were grown in Rosewell Park Memorial Institute medium (RPMI) with 10% FBS and 1% P/S. H9c2 cells were treated with 10 μM doxorubicin (dox; Sigma-Aldrich, St. Louis, MO) for 12 h to induce apoptosis. NSCLC cell lines (A549, H2009, H1299, and Calu-1) were treated with various concentrations of apigenin (Sigma-Aldrich), ranging from 1 to 50 μM, and/or human recombinant TRAIL (EMD Millipore, Billerica, MA), ranging from 25 to 100 ng/ml.

2.4 Cell Viability Assays

Cell viability was determined using the CellTiter 96® Aqueous One Solution Cell Proliferation Assay (MTS; Promega, Madison, WI). Cells were seeded in a 96-well plate at a density of 8,000 cells/75 μl media/well. Twelve hours later, cells were treated with 1, 10, 25, and 50 μM apigenin or DMSO-diluent control for 24 h. Next, 25, 50, or 100 ng/ml TRAIL or TRAIL Buffer alone was added and cells were cultured for an additional 24 h. The MTS

reagent was added and cells were incubated for 2 h at 37°C before measuring the absorbance at 490 nm on a multi-plate reader VICTOR™ X3 (Perkin Elmer, Waltham, MA).

2.5 Flow Cytometry

The percentage of apoptosis was analyzed using the Annexin V Apoptosis Detection Kit (BD Biosciences, San Jose, CA). Briefly, 2.5 x 10^5 cells were stained in 0.1 ml of Annexin V binding buffer containing 1% FBS, 1 µg Annexin V-APC, 0.5 µg 7-AAD for 20 min on ice. Cells were rinsed with 0.5 ml of Annexin V staining buffer and centrifuged at 1,200 rpm at 4°C for 5 min. Cell pellets were resuspended in 0.1 ml of Cytofix/Cytoperm™ (BD Biosciences, San Jose, CA), incubated for 20 min on ice, washed twice with 0.5 ml of the Annexin V staining buffer, and spun at 1,200 rpm at 4°C for 5 min. Pellets were resuspended with 0.1 ml of permeabilization solution containing either 1 µg of anti-IgG isotype control-FITC or anti-active-caspase-3-FITC antibodies. Cells were rinsed twice with 0.5 ml in Annexin V staining buffer, spun at 1,200 rpm at 4°C for 5 min, and resuspended in 0.5 ml of Annexin V staining buffer containing 1% paraformaldehyde. Samples were then analyzed by flow cytometry.

2.6 Transient Transfection

Eight million HeLa or H9c2 cells in 5 ml of media were transiently transfected with 8 µg of DNA using 15 µl of Lipofectamine 2000 (Invitrogen) and incubated for 4 h at 37°C in 5 ml of serum-free DMEM. Following incubation, 5 ml of DMEM containing 20% FBS was added and cells were cultured for an additional 8 h. Twenty-four hours after transfection samples were collected by detaching cells using 0.05% Trypsin-EDTA (Invitrogen,

Carlsbad, CA) for 5 min at 37°C, transferred to Falcon tubes, and centrifuged at 1,200 rpm for 5 min. Cells were washed with 0.5 ml PBS, transferred to an eppendorf tube, and centrifuged at 6,000 rpm for 5 min at 4°C. Cell pellets were snap-frozen in liquid nitrogen and stored at -80°C.

2.7 Western Blot Analysis

HeLa lysates were prepared by resuspending cell pellets in Lysis Buffer B (50 mM HEPES pH 7.5, 2.5 mM EGTA, 1 mM EDTA, 150 mM NaCl, 10% glycerol, 0.1% Tween-20 containing 50 mM NaF, 10 mM Na-glycerophosphate, 5 mM Na-pyrophosphate, 1 mM Na-orthovanadate, 1 mM DTT, 1 mM PMSF, and 2 μg/mL protease inhibitors: chymostatin, leupeptin, antipain, and pepstatin). H9c2 and NSCLC cell lysates were resuspended in NP-40 lysis buffer (10 mM Tris-Cl, pH 7.5, 0.5% (v/v) NP-40, 1 mM DTT, 0.1 mM PMSF, 2 μg/ml protease inhibitors) for 1 h at 4°C under constant vortexing. Lysates were centrifuged for 5 min at 13,200 rpm at 4°C and supernatants were stored at -80°C. Protein concentration was determined by mixing 1 μl of lysate with 199 μl of 1 x Bradford Protein Assay reagent (Bio-Rad, Hercules, CA) for 5 min at room temperature. Absorbance was measured at 595 nm and protein concentration was calculated using a standard curve of 0, 1, 2, 4, 6, 8, and 10 μg BSA. Samples were measured on a 96-well plate using the multi label plate reader VICTOR™ X3 (Perkin Elmer).

Equal amounts of protein were heated at 95°C for 5 min in SDS loading buffer (250 mM Tris, pH 6.8, 10% SDS, 50% glycerol, 0.5% bromophenol blue, and 1.78 M 2-mercaptoethanol). Protein samples, along with the SeeBlue® Plus Marker (Invitrogen), were resolved by SDS-PAGE on a 12% gel by running at 100 V for 10 min followed by 160 V

for 90 min. Separated polypeptides were transferred to nitrocellulose membranes (0.20 μm, Whatman, USA) at 250 mA for 75 min at room temperature using transfer buffer (25 mM Tris, pH 8.3, 192 mM glycine, 20% methanol). The membranes were blocked with 5% BSA in TBS-T buffer (10 mM Tris, pH 7.6, 150 mM NaCl, 0.05% Tween-20) for 30 min. Primary and secondary antibodies (Table 3) were diluted to working concentrations in 0.25% BSA in TBS-T buffer. Membranes were incubated with primary antibodies at 4°C for 12 h followed by 3 washes with TBS-T. Secondary antibodies conjugated to horseradish peroxidase were added to the membranes for 1 h at room temperature followed by 3 more washes with TBS-T. Proteins were visualized using the HyGLO™ Chemiluminescent HRP Detection Reagent (Denville Scientific, Metuchen, NJ).

Table 3. List of Antibodies

Antibody	Clone	Type	Catalog Number	Company	Location
anti-caspase-3	19	monoclonal	610323	BD Biosciences	San Jose, CA
anti-active-caspase-3-FITC	-	monoclonal	559341	BD Biosciences	San Jose, CA
anti-Bid	FL-195	polyclonal	SC11423	Santa Cruz	Santa Cruz, CA
anti-DR5	-	polyclonal	AB16942	Millipore	Billerica, MA
anti-GAPDH	FL-355	polyclonal	SC25778	Santa Cruz	Santa Cruz, CA
anti-Hsp27	-	polyclonal	SPA803	Assay Designs	Ann Arbor, MI
anti-Hsp70	C92F3A-5	monoclonal	SPA810	Assay Designs	Ann Arbor, MI
anti-IgG	-	monoclonal	SC2025	Santa Cruz	Santa Cruz, CA
anti-IgG	-	polyclonal	SC2027	Santa Cruz	Santa Cruz, CA
anti-IgG-FITC	-	polyclonal	555786	BD Biosciences	Billerica, MA
anti-IgG-PE	G18-145	polyclonal	555787	BD Biosciences	Billerica, MA
anti-myc	9E10	monoclonal	SC40	Santa Cruz	Santa Cruz, CA
anti-XIAP	28	monoclonal	610717	BD Biosciences	San Jose, CA
anti-β-Tubulin	AA2	monoclonal	SC80011	Santa Cruz	Santa Cruz, CA
anti-mouse-HRP	-	monoclonal	NA931V	GE Healthcare	Buckinghamshire, UK
anti-rabbit-HRP	-	polyclonal	NA934V	GE Healthcare	Buckinghamshire, UK

2.8 Immunoprecipitation

For immunoprecipitations (IP) of myc-tagged Hsp27 chimera proteins, 5 x 10^6 HeLa cells, transiently transfected as described in section 2.8 were lysed in Lysis Buffer B for 1 h at 4°C. One milligram of cell lysate was immunoprecipitated using 1 µg of anti-myc antibodies or anti-IgG isotype control antibodies (Table 3), in a total volume of 0.5 ml, and incubated in a 360° rotator overnight at 4°C. The IPs were then incubated with 30 µl Protein G-Agarose beads (Invitrogen, Carlsbad, CA) for 1 h at 4°C. The mixtures were washed four times with 500 µl of Lysis Buffer B. IPs were resuspended in 20 µl of 2 x SDS loading buffer and heated at 95°C for 5 min. Western Blot analysis was performed as described in section 2.7.

For immunoprecipitations of endogenous DR5, 5 x 10^6 of NSCLC cells were lysed in 1 ml of ice cold 1% NP-40 buffer (10 mM Tris-Cl, pH 7.5, 1% (v/v) NP-40, 1 mM DTT, 0.1 mM PMSF, 2 µg/ml protease inhibitors) for 2 h at 4°C. One milligram of cell extracts was immunoprecipitated in a total volume of 0.5 ml using 1 µg of anti-IgG isotype control or anti-DR5 antibodies (Table 3). Reactions were incubated for 14 h at 4°C and mixed with 30 µl of Protein G-Agarose beads. IPs were incubated for 1 h at 4°C, rinsed four times with 0.7 ml of 1% NP-40 buffer, and resuspended in 30 µl of 2 x SDS loading buffer and heated at 95°C for 5 min. Western Blot analysis was performed as described in section 2.7.

2.9 Caspase Activity Assays

Caspase-3, -8, and -9 activity was determined using the fluorescent substrates Ac-Asp-Glu-Val-Asp-AFC (DEVD-AFC), Ac-Ile-Glu-Thr-Asp-AFC (IETD-AFC), and Ac-Leu-Glu-

His-Asp-AFC (LEHD-AFC), respectively (Enzo Life Sciences, Farmingdale, NY). Cell lysates were incubated in the appropriate reaction buffer (caspase-3 buffer: 10% glycerol, 50 mM PIPES, pH 7.0, 1 mM EDTA, 1 mM DTT, 20 μM DEVD-AFC; caspase-8 buffer: 100 mM HEPES, pH 7.5, 10% (w/v) sucrose, 1 mM EDTA, 1 mM DTT, 20 μM IETD-AFC; caspase-9 buffer: 100 mM MES, pH 6.5, 10% (w/v) PEG, 0.1% (w/v) CHAPS, 1 mM DTT, 20 μM LEHD-AFC). The release of free AFC was measured using a Cytofluor 4000 fluoromter (Perspective Co., Farmingham, MA; excitation 400 nm, emission 508 nm). For each reaction, 20 μg of cell lysates were mixed with reaction buffer to a total of 200 μl and fluorometer measurements were taken every 30 sec for 1 h.

2.10 Protein Purification

2.10.1 Purification of Hsp27

An individual bacteria colony containing pQE32-Hsp27 plasmid DNA (AB 374, Table 1) was grown in Terrific Broth (2.4% yeast extract, 1.2% tryptone, 4% glycerol, 0.17 M KH_2PO_4, 0.72 M K_2HPO_4) to an OD_{600} of approximately 0.5. Protein expression was induced with 1 mM IPTG for 3 h at 37°C. Cells were collected and 2 g of the bacterial pellet was resuspended in 20 ml denaturing buffer (100 mM NaH_2PO_4, pH 8.0, 10 mM Tris and 8 M urea) and incubated for 30 min at room temperature. Cells were sonicated (output: 8, duty cycle: 80, utilizing the Sonifier 450, Branson Ultrasonics, Danbury, CT) and lysates were incubated with 250 μl of Ni^{2+}-NTA beads (Qiagen) for 90 min at room temperature in the presence of 1 μl/mL RNase and DNase. The lysate-bead mixture was loaded onto an empty column and the flow-through was collected. The beads were washed twice with 5 ml Buffer C (100 mM NaH_2PO_4, 10 mM Tris, 8 M urea, 1 μl/mL RNase and DNase, pH 6.3).

Elutions were collected with 5 ml Buffer D (100 mM NaH_2PO_4, 10 mM Tris, 8 M urea, 1 µl/mL RNase and DNase, pH 5.9) and 5 ml Buffer E (100 mM NaH_2PO_4, 10 mM Tris, 8 M urea, 1 µl/mL RNase and DNase, pH 4.5), and elution fractions containing Hsp27 proteins were identified by SDS-PAGE and staining with Coomassie solution (0.25% (w/v) Coomassie brilliant blue R-250, 50% (w/v) methanol, 10% (v/v) glacial acetic acid) at room temperature. The denatured proteins were refolded by a stepwise dialyzing procedure, first for 3 h at room temperature in dialysis buffer 1 (25 mM NaH_2PO_4, 100 mM NaCl, 1% glycerol, 0.1 mM PMSF) with the ratio of 1 ml protein to 1000 ml dialysis buffer 1. Next, protein samples were dialyzed for 12 h at 4°C in dialysis buffer 1 with the same protein:buffer ratio. Precipitated proteins were removed by centrifugation for 10 min at 4,000 rpm and supernatants were then dialyzed for 12 h at 4°C in dialysis buffer 2 (20 mM Tris, pH 7.4, 10 mM NaCl, 1 mM EDTA, 1 mM DTT, 0.1 mM PMSF) using the same protein:buffer ratio. Protein yield was determined by Bradford assay, as described in section 2.7.

2.10.2 Purification of Caspase-3

An individual bacteria colony containing pQE31-caspase-3 plasmid DNA (AB 441, Table 1) was grown in Terrific Broth to an OD_{600} of approximately 0.5. Protein expression was induced with 1 mM IPTG for 30 min at 20°C. Cells were collected and lysed via sonication (output: 8, duty cycle: 80, utilizing the Sonifier 450) in sonication buffer (50 mM sodium phosphate, pH 7.8, 300 mM NaCl, 5 mM 2-mercaptoethanol, 1% Tween-20, 2 µg/mL protease inhibitors, and 1 mM PMSF). Lysates were centrifuged at 12,000 rpm for 10 min and the supernatants were treated with 10 µg/ml RNase and 5 µg/ml DNase for 10

min at 4°C. Supernatants were incubated with 125 µl of Ni^{2+}-NTA beads (Qiagen) for 90 min at 4°C. The lysate-bead mixture was loaded onto an empty column and the flow-through was collected. The beads were washed once with 10 ml of washing buffer (50 mM HEPES, pH 7.4, 50 mM NaCl, 10% glycerol, 1% Tween-20, 0.1 mM PMSF, 2 µg/ml protease inhibitors). Elutions were collected in washing buffer with concentrations of imidazole of 30, 50, and 100 mM, and elution fractions containing caspase-3 proteins were identified by SDS-PAGE and gels were stained with Coomassie staining as described in section 2.10.1. Fractions containing caspase-3 were dialyzed twice in caspase-3 reaction buffer (50 mM HEPES, pH 7.4, 50 mM NaCl, 10% (w/v) sucrose, 1 mM DTT, 0.1 mM PMSF) for 3 h at 4°C with 1 ml of protein for 1000 ml of buffer. Protein yield was determined by Bradford assay, as described in section 2.7.

2.11 Structural Modeling

The Swiss Model program (http://swissmodel.expasy.org) was used to generate Hsp27 models based on sequence homology with crystallized proteins submitted to the Protein Data Bank (PDB). Oligomeric structures were built by modeling Swiss Model structures on fully crystallized sHsps and aa accessibility was calculated using the Deep View program (http://spdbv.vital-it.ch, version 4.04). The accessibility scale included with each figure is approximate and ranges from a completely buried aa (dark blue) to an aa that is at least 65% accessible (red).

2.12 Isobolograms

Isobolograms were generated from NSCLC combination treatments by calculating the IC_{50} of each treatment alone to graph the line of additivity. Combination treatments were graphed as points on the plots, along with the calculated Combination Index (CI) using the following formula:

$$CI = \frac{D_A}{(IC_{50})_A} + \frac{D_B}{(IC_{50})_B}$$

Where $(IC_{50})_A$ is the concentration of drug A alone needed for a 50% effect, $(IC_{50})_B$ is the concentration of drug B alone needed for a 50% effect, and D_A and D_B are the concentrations of drug A and B used in the combination treatment for a 50% effect.

2.13 Statistical Analysis

All experiments were done in biological triplicates and the data presented represent the mean of experimental repeats with differences calculated as standard error of the mean (SEM). The SEM was calculated by dividing the standard deviation (STD) by the square root of the number of repeats (n).

$$SEM = \frac{STD}{\sqrt{n}}$$

Statistical significance was calculated by two-way ANOVA for NSCLC drug combination experiments and by using the student's *t*-test for all other experiments with significance expressed as *p*-values.

Chapter 3

Role of Hsp27 in the Regulation of Caspase-3 Activation

3.1 Introduction

Various chemotherapy drugs have been shown to induce apoptosis in cancer cells through the intrinsic pathway involving mitochondrial release of cytochrome C and activation of caspase-9 (23,73-75). Included in this group are the anthracyclines, tetracyclic compounds originally isolated from the Gram-negative bacteria *Streptomyces peuceticus*, and considered to be some of the most effective chemotherapeutic agents, used in the treatment of many cancers including breast cancers, soft tissue sarcomas, lymphomas, and acute lymphoblastic and myeloblastic leukemia (Fig. 2) (76-81). However, adverse cytotoxic effects are associated with these drugs (82). Doxorubicin (dox), one of the most commonly used anthracyclines, functions by intercalating DNA and inducing apoptosis caused by promoting DNA damage (Fig. 2A) (76). The anthracyclines danorubicin, epirubicin, and idarubicin function similarly, but have been shown to be less effective than dox (Fig. 2B, C, and D) (76). However, anthracyclines, including dox, cause dilated cardiomyopathy (weakening and enlarging of the heart muscle) and congestive heart failure in 30% of patients with a mortality rate of 30-50% (76). Cardiovascular diseases resulting from the treatment with dox are caused by cardiomyocyte death, which is the result of dox-induced ROS production that leads to the initiation of apoptosis (22). However, the mechanisms that regulate dox-mediated cardiomyocyte apoptosis remain unclear. Due to the high mortality rate, identifying novel approaches to reduce the cardiotoxicity of dox treatment is of great importance.

Hsp27 has emerged as an inhibitor of apoptosis by preventing the mitochondrial release of cytochrome C and inhibiting caspase-3 activity (21,46). Over-expression of Hsp27 has been detected in many cancer cells and human cancer biopsies, and it has been suggested to be a useful prognostic marker (2,83,84). In addition, Hsp27 has been suggested to act as a key inhibitor of apoptosis in the rat cell line H9c2, a well-accepted model to study cardiomyocyte biology (85-87). The H9c2 cell line is derived from embryonic rat hearts and retains many features of cardiac muscle including the cardiac isoform of creatine phosphokinase, L-type Ca^{2+} channels, and the tissue-specific splicing protein survival of motor neuron (SmN), and is therefore a commonly used model system to study cardiomyocyte life span (88,89). It has been shown that increased temperature induces Hsp27 expression in H9c2 cells, and this increased expression is able to block dox-induced apoptosis (82). Studies further demonstrated that chemotherapy drugs, such as cisplatin or gemcitabine, can increase Hsp27 expression, thereby conferring greater chemo-resistance (90). Our group previously showed that Hsp27 associates with caspase-3 in cells of the immune system preventing its activation during apoptosis (21). It is hypothesized that many protein-protein interactions are mediated by the α-crystallin domain of Hsp27 (Fig. 3A). However, the mechanism by which Hsp27 controls caspase-3 and its role in the inhibition of dox-induced apoptosis has not been characterized.

In this study, the Hsp27 peptide region responsible for the association with caspase-3 was identified and shown to be capable of inhibiting apoptosis. Hsp27 nested deletion clones were generated by PCR and cloned into mammalian expression vectors. The clones were subsequently expressed in cells and it was determined which clones were unable to bind to caspase-3 by immunoprecipitations. Our results showed that two subdomains of

Hsp27 between aa 104-119 and 154-186 seem to contribute to the binding to caspase-3. In parallel, protein-modeling software was utilized to generate an Hsp27 structure based on the evolutionarily related archaean Hsp16.5 (91). The Hsp16.5 structure was used to obtain an Hsp27 model, since the Hsp27 crystal structure has not yet been resolved, to aid in the explanation of how the deletions are likely involved in the interaction with caspase-3. Finally, our studies further showed that a loss of Hsp27 binding to caspase-3 resulted in decreased protection from dox-induced apoptosis.

3.2 Identification of the Hsp27 Peptide Region Responsible for the Association with Caspase-3

To determine the Hsp27 region that is directly involved in the association with and inhibition of caspase-3, several Hsp27 clones lacking specific domains were generated. Initially, N-terminal myc-tagged clones of the full-length Hsp27 wt (Hsp27-FL), Hsp27 N-terminal, and Hsp27 C-terminal were cloned into a mammalian expression vector (Tables 1 and 2; Fig. 3B). For this purpose, the Hsp27-FL clone (AB 262, Table 1 and Fig. 5A) was used as a template to generate Hsp27 N-terminal using the primers PAO 356 and 565 and Hsp27 C-terminal using PAO 564 and 357 (Tables 1 and 2). The obtained Hsp27 DNA fragments were cloned into the *BamH*I/*Xho*I sites of the pCDNA3-5 x myc mammalian expression vector, which carries an N-terminal myc-epitope tag and allows for expression in mammalian cells.

The clones were transiently transfected in HeLa cells and cell lysates were used in western blot analyses to determine that the clones were expressed at similar levels and that the proteins were of the proper size (Fig. 3B, Input). To study the association with

caspase-3, the lysates were immunoprecipitated (IP) with anti-caspase-3 antibodies or an anti-IgG isotype control (Fig. 3B, lane 1). The IPs were resolved by SDS-PAGE, transferred to nitrocellulose, and proteins were detected by immunoblotting with anti-myc and anti-caspase-3 antibodies (Fig. 3B). Our results showed that the Hsp27-FL and the Hsp27 C-terminal were able to bind to caspase-3 (Fig. 3B, lanes 3 and 4), while the Hsp27 N-terminal was not able to associate with caspase-3 (Fig. 3B, lane 2), even though all clones were expressed at similar levels as shown by the input (Fig. 3B, lanes 5-7). These results suggest that the C-terminal domain of Hsp27 is sufficient to bind to caspase-3.

To determine whether the Hsp27 C-terminal domain is likewise able to regulate caspase-3 activity, we performed caspase activity assays using purified human recombinant 6 x His-tagged Hsp27 proteins containing different domains: rHsp27-FL, rHsp27 C-term, and rHsp27 N-term (Fig. 3C). Hsp27 proteins were obtained by cloning the Hsp27 DNA fragment of interest into the pQE32 bacterial expression vector and proteins were purified from *E. coli* lysates as described in section 2.10.1. Recombinant human caspase-3 (rCasp-3) was incubated with the rHsp27 proteins and the complex was allowed to form for 30 min at 4°C. Next, recombinant active-caspase-9 (rCasp-9) was added to induce the activation of caspase-3 for up to 2 h at 37°C. Caspase-3 activity was determined by following the release of fluorescence upon the cleavage of the DEVD-AFC substrate (Fig. 3C). The rHsp27-FL and rHsp27 C-term domains were both able to inhibit caspase-3 activity at a similar level, while rHsp27 N-term was unable to prevent its activity at a level similar to that observed in the absence of Hsp27 (Fig. 3C). In addition, the processing of caspase-3 was followed by western blot analyses using anti-caspase-3 antibodies, which recognize an epitope on the p17 subunit of caspase-3 to distinguish the precursor (inactive

enzyme) as well as smaller subunits (prop17 and p17) that present when the enzyme is active (Table 3; Fig. 3D). Similar to the activity assay, after 2 h of incubation the immunoblots showed that rHsp27 N-term allows for caspase-3 proteolytic processing and formation of the free p17 subunit, while rHsp27-FL and rHsp27 C-term inhibit caspase-3 activation at the autocatalytic cleavage of the prodomain (Fig. 3D).

Based on our previous results, it was hypothesized that the Hsp27 peptide region responsible for the association with caspase-3 is located within the C-terminal domain. To define a smaller peptide region capable of inhibiting the association with and activity of caspase-3, a series of myc-tagged Hsp27 nested deletion clones were generated (Fig. 5A). The size of each successive deletion was based on the conserved secondary structure of several evolutionarily related Hsp27 proteins from various species with deletions occurring adjacent to whole β-sheets or α-helices (Fig. 4). Five deletion clones were generated that encode for Hsp27 Δ187-205 and deletion of the C-terminal extension, Hsp27 Δ154-205 and deletion of β8 and β9, Hsp27 Δ137-205 and deletion of β7 and α2, Hsp27 Δ120-205 and deletion of β5 and α1, and Hsp27 Δ104-205 and deletion of β4 (Fig. 4). The Hsp27-FL clone (AB 262, Table 1) was used as a template to generate the Hsp27 nested deletion clones by PCR. The primers PAO 356 and 559 were used to generate Hsp27 Δ187-205, PAO 356 and 560 for Hsp27 Δ154-205, PAO 356 and 561 for Hsp27 Δ137-205, PAO 356 and 562 for Hsp27 Δ120-205, and PAO 356 and 563 for Hsp27 Δ104-205 (Tables 1 and 2). The PCR products were run on agarose gels and were found to be of the expected 558 bp for Hsp27 Δ187-205, 459 bp for Hsp27 Δ154-205, 408 bp for Hsp27 Δ137-205, 357 bp for Hsp27 Δ120-205, and 309 bp for Hsp27 Δ104-205 (Fig. 5B). After sequencing the PCR products to ensure accuracy of the mutant, the Hsp27 inserts were

subcloned into the myc-tagged mammalian expression vector. Samples were screened for the presence of the insert using restriction enzyme analysis with *BamH*I and *Xho*I, and the same expected insert sizes as described above as well as the myc-vector of 5500 bp were obtained (Fig. 5C).

To determine the subdomain of Hsp27 required for the association with caspase-3, the obtained myc-tagged Hsp27 deletion clones were transiently transfected in HeLa cells. Western blot analyses with anti-myc antibodies showed equal expression of proteins of the proper size were obtained (Fig. 6, Input). To determine the subdomain of Hsp27 required for the association with caspase-3, the lysates were immunoprecipitated (IP) with anti-myc antibodies or an anti-IgG isotype control (Fig. 6, lane 1). The IPs were resolved by SDS-PAGE and proteins were detected by immunoblotting with anti-myc and anti-caspase-3 antibodies (Fig. 6, lanes 1-9). Hsp27 Δ187-205 was able to associate with caspase-3 similar to Hsp27-FL (Fig. 6, lanes 2 and 3). The deletion of Hsp27 Δ154-205 (clone C) showed a decrease of binding to caspase-3 of about 50%, levels similar to lysates expressing the deletions Hsp27 Δ136-205 and Hsp27 Δ120-205, corresponding to clones D and E, respectively (Fig. 6, lanes 4-6). Binding to caspase-3 was completely abolished when Hsp27 aa 104-119 were deleted (clone F) (Fig. 6, lane 7). Collectively, these results suggest that aa 154-186 and aa 104-119 contribute to the association with caspase-3.

3.3 The Role of Hsp27 in the Regulation of Caspase-3 in Cardiomyocytes

To investigate the amino acids of Hsp27 that regulate the activity of caspase-3 during apoptosis, the H9c2 cell line was used as a cardiomyocyte model (Fig. 7E). H9c2s were transiently transfected with the Hsp27 nested deletion clones, and 16 h after

transfection, apoptosis was induced by treating with 10 μM dox for 12 h. The percentage of apoptotic and active caspase-3 positive cells was determined by flow cytometry after staining with Annexin-V/7AAD and anti-caspase-3-FITC antibodies, respectively (Fig. 7A and B). All nested deletion clones except for Hsp27 Δ104-205 were able to reduce apoptotic cells and active caspase-3^+ cells by about 75% (Fig. 7A and B, bars A-E). Overexpression of Hsp27 Δ104-205 resulted in apoptotic and active caspase-3^+ cell levels similar to the empty myc-vector control (Fig. 7A and B, bar F).

In addition, the enzymatic activity of caspase-3 and -9 was determined in the same samples using the DEVD-AFC and LEHD-AFC assays, respectively (Fig. 7C and D). Caspase-3 activity was significantly inhibited by about 50% by all deletions except for Hsp27 Δ104-205 (clone F) (Fig. 7C, bars A-E). However, although caspase-9 activity was still inhibited by about 40% through deletions of Hsp27 aa 154-205 (Fig. 7D, bars A-C), beginning with Hsp27 Δ137-205, caspase-9 inhibition lost statistical significance and was gradually restored with each successive deletion (Fig. 7D, bars D-F).

Altogether, these results show that Hsp27 Δ154-205 has decreased binding to caspase-3 but is still able to inhibit apoptosis. In addition, Hsp27 Δ104-205 is not able to bind to caspase-3 and does not inhibit caspase-3 activity or apoptosis, suggesting that the loss in binding of Hsp27 Δ154-205 to caspase-3 is not essential for its ability to prevent caspase-3 activity. This could occur if the reduced binding was still sufficient to prevent caspase-3 activation or if Hsp27 Δ154-205 is still able to inhibit the apoptotic signaling cascade upstream of caspase-3.

3.4 Structural Prediction of Hsp27-Caspase-3 Interaction

The regions of Hsp27 between aa 104-119 and aa 154-186 were both found to be potential binding domains for the inhibition of caspase-3 activity. To better understand this mechanism, structural features within each domain that could contribute to protein-protein interactions were studied based on protein crystal structures. A limitation of this approach however is that human Hsp27 has not yet been successfully crystallized. So far, only four complete evolutionarily related sHsp structures have been resolved by x-ray crystallography (91-94). Hsp16.5 is an archaean protein purified from *Methanococcus janaschii*, which was the first crystallized sHsp and shares 15% sequence homology with Hsp27 (91). The protein consists of 24 monomers arranged in a roughly spherical shape (Fig. 8A). The wheat (*Triticum aestivum*) Hsp16.9 is made of 12 monomers that form two back-to-back hexameric rings and is 17% similar to Hsp27 (Fig. 8B), while the Tsp36 is a flatworm (*Taenia saginata*) sHsp that forms a functional dimer and is 25% homologous to Hsp27 (Fig. 8C) (92,94). The most recent sHsp to be crystallized is the bacterial (*Xanthomonas axonopodis*) sHspA, which shares 17% sequence identity with Hsp27 (93). Although the protein forms a functional 36-mer, only the dimer structure is currently available through the Protein Data Bank for analysis (Fig. 8D).

Each of the crystallized sHsps was assessed for its ability to serve as a model for Hsp27 quaternary structure by comparing sequence and secondary structure homology information available in the literature. The bacteria sHspA was not included in the analysis as its full structure is not yet available. Several key features define a sHsp including the presence of a α-crystallin domain, the formation of a homodimer in an anti-parallel orientation, and the formation of large oligomeric structures using the homodimers as

building blocks (40). The monomers of Tsp36 only form dimers in a perpendicular orientation, and each monomer contains two α-crystallin domains (94). However, Hsp27 has been shown to form anti-parallel dimers and oligomeric structures as large as 400 kDa, and it contains only one α-crystallin domain (95,96). Due to the structural discrepancies between Hsp27 and Tsp36, the flatworm protein would not serve as a good model for Hsp27 structure and was therefore excluded from further analysis. The remaining two structures, Hsp16.5 and Hsp16.9, posess the typical features of a sHsp described above and are very structurally similar. The two proteins do however differ on the number of residues between their ninth and tenth β-strands, which is believed to be important in the determination of quaternary structure (41). Hsp16.9 has more residues between β9 and β10, which leads to the formation of a "hinge" that is crucial for its oligomeric structure (92). Hsp16.5 has fewer aa between the same two strands and is therefore unable to form a similar "hinge," resulting in a very different quaternary structure (91). Hsp27 has few residues between β9 and β10, suggesting that it may develop an oligomeric structure similar to that of Hsp16.5. Therefore, we chose to utilize Hsp16.5 as a model of Hsp27 structure.

In order to examine the structural features of Hsp27, the Swiss Model program was used to generate an Hsp27 model based on the model of Hsp16.5 (Fig. 9A). In addition, the Deep View program was utilized to calculate the accessibility of the aa within the α-crystallin domain (Fig. 9B). Analyzing known binding domains of other proteins revealed that aa require at least 25% accessibility for protein-protein interactions, as calculated by Deep View. Within the first potential caspase-3 binding region that contains aa 104-119 (Fig. 9, yellow) most of the residues are buried, though aa 104-106 are accessible enough

for protein-protein interactions (Fig. 9, purple). Interestingly, within the structure this corresponds to a small loop that rises away from the surface of the protein (Fig. 9A, purple). The second potential caspase-3 binding region, aa 154-186, contains numerous regions of accessibility, though it lacks a loop, groove, or other obvious structures for protein-protein interactions (Fig. 9A, white). Due to the limitations of using the structure of Hsp16.5 as a model, Hsp27 aa 187-205 are unaccounted for since Hsp16.5 is comprised of just 147 aa, and their presence could lower the accessibility of the aa within the second potential caspse-3 binding region. Altogether, these results support the hypothesis that Hsp27 aa 104-119 and aa 154-186 are important for the association with caspase-3.

3.5 Conclusion

This study investigated the interaction between Hsp27 and caspase-3 to define the Hsp27 peptide region essential for the inhibition of caspase-3 activation during apoptosis. Using Hsp27 deletion clones, we were able to define that the binding region is possibly aa 104-119, aa 154-186, or contributed to by both aa regions. We discovered that while loss of aa 154-186 causes a reduction in Hsp27 association to caspase-3, Hsp27 is still able to inhibit caspase-3 activity and apoptosis in cardiomyocytes. This may indicate that aa 154-186 is a non-essential binding region or that Hsp27 Δ154-205 is still able to inhibit apoptosis upstream of caspase-3 activation. Furthermore, Hsp27 protection of cardiomyocytes from dox-induced apoptosis and caspase-3 activity is not lost until the deletion of aa 104-119, suggesting this region is vitally important to the execution of apoptosis mediated by caspase-3. To further investigate Hsp27 structural features that could contribute to protein-protein interactions, we utilized Hsp16.5 as a model for

quaternary structure. We analyzed the accessibility of Hsp27 aa modeled after Hsp16.5 and found that aa regions 104-119 and 154-186 both contain residues accessible enough for protein-protein interactions. These results suggest that Hsp27 regulates caspase-3 activation through an interaction between Hsp27 aa 104-119 and 154-186 and the prodomain of caspase-3. This study contributes to the understanding of the mechanism by which Hsp27 inhibits caspase-3 activity and will lead to the development of a peptide therapy to prevent cardiomyocyte apoptosis during dox treatment.

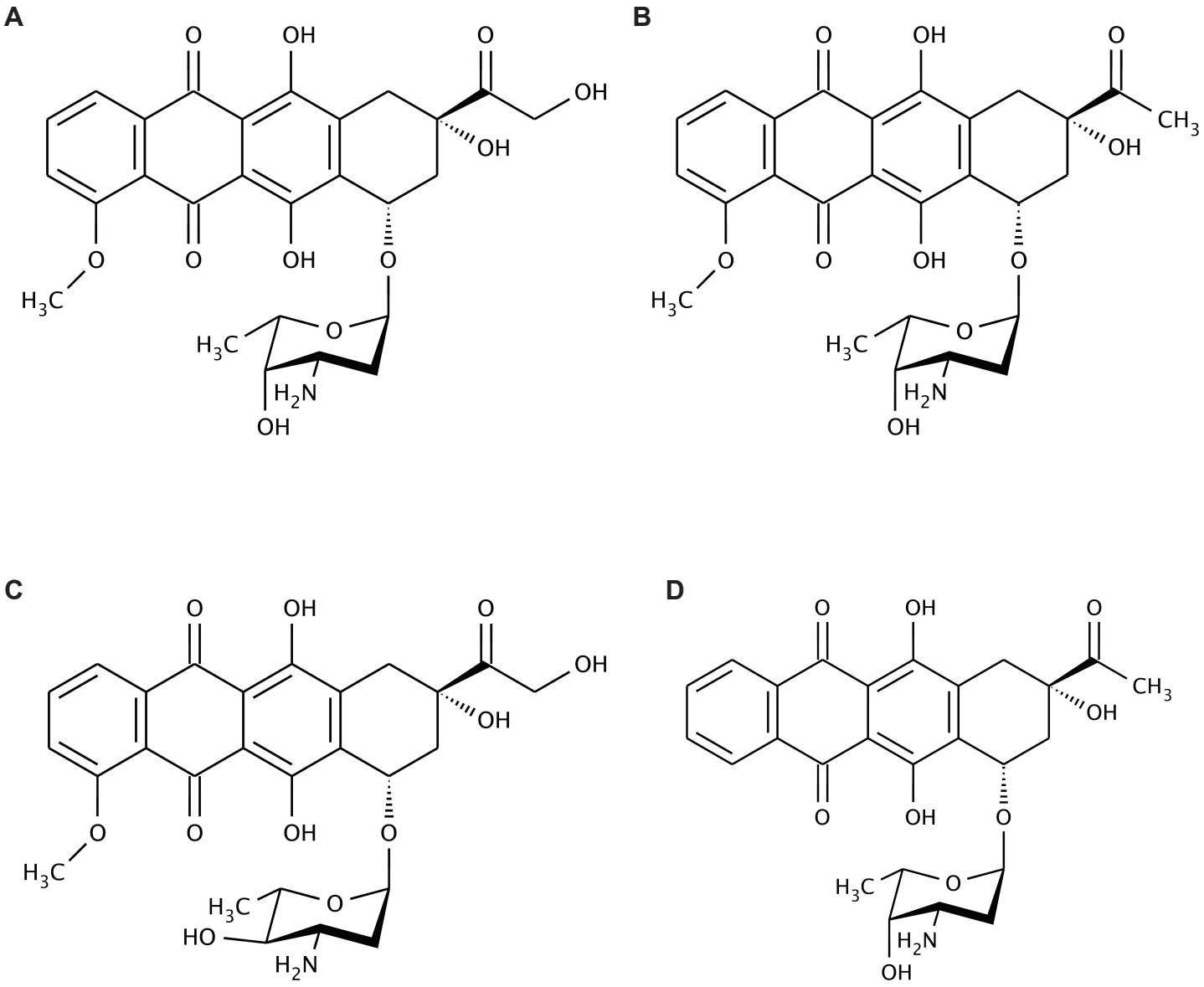

Figure 2. Structures of some common anthracyclines. A: Doxorubicin (dox), one of the first isolated anthracyclines and the most commonly used for the treatment of many cancers. **B:** Danorubicin (dan), one of the first isolated anthracyclines. **C:** Epicubicin, an analog of dox. **D:** Idarubicin, an analog of dan.

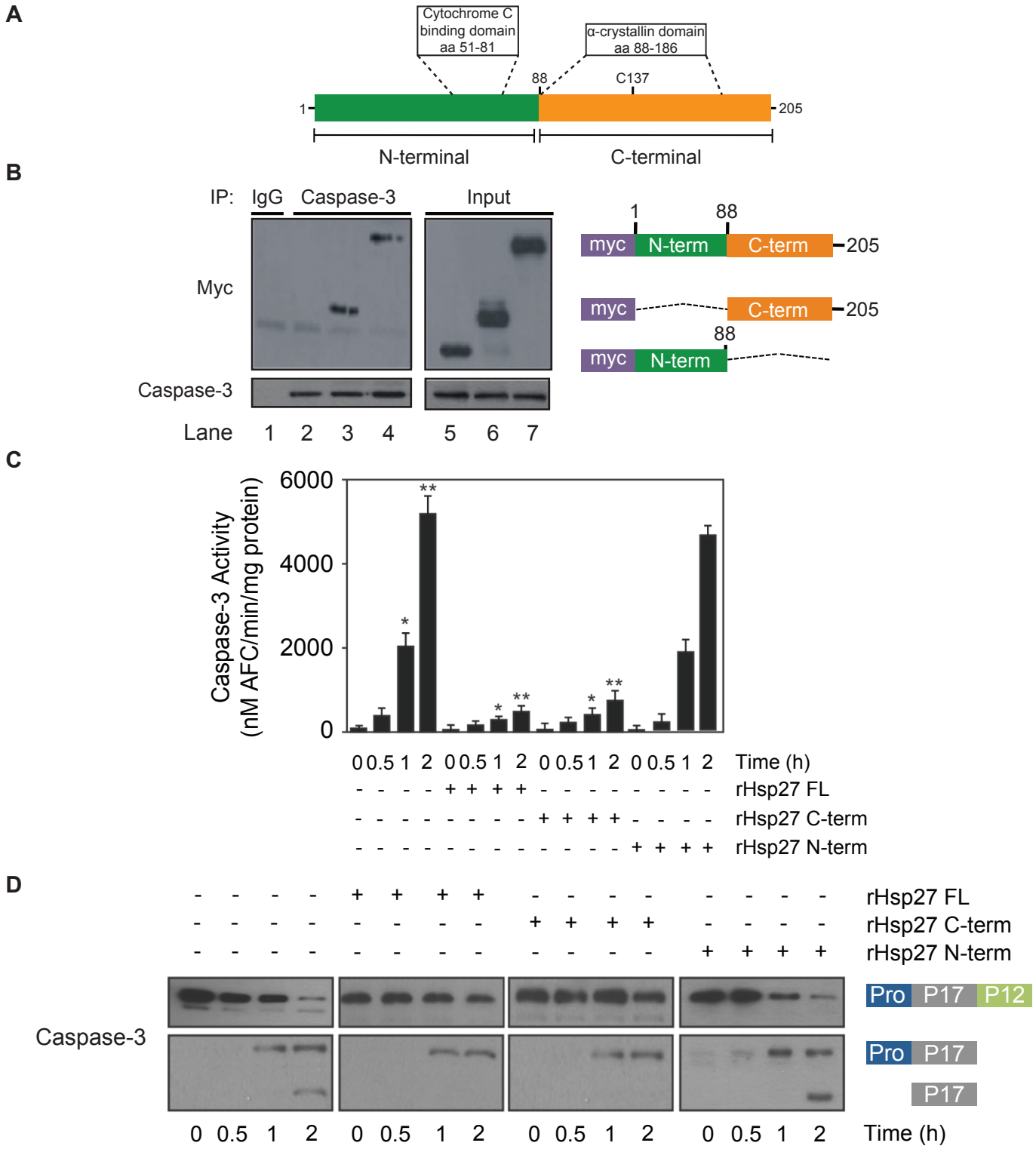

Figure 3. Hsp27 C-terminal associates with caspase-3 to inhibit its activity. **A:** Schematic representation of human Hsp27. **B:** Extracts from HeLa cells transiently transfected with myc-tagged Hsp27 FL, N-term, or C-term were immunoprecipitated (IP) with anti-caspase-3 antibodies or an isotype control (lane 1). IPs were analyzed by immunoblotting with anti-myc and anti-caspase-3. **C-D:** Purified human recombinant 6 x His-tagged caspase-3 and 6 x His-tagged Hsp27 were incubated for 30 min at 4°C. Following the caspase-3:Hsp27 complex formation, recombinant active-caspase-9 was added to induce the first cleavage of caspase-3. Caspase-3 activity was determined by the DEVD-AFC activity assay, while the processing of caspase-3 was followed by western blot analysis using anti-caspase-3 antibodies. Results were obtained from three independent experiments and are expressed as means ± SEM (n=3) Panels B-D are courtesy of Dr. Oliver Voss.

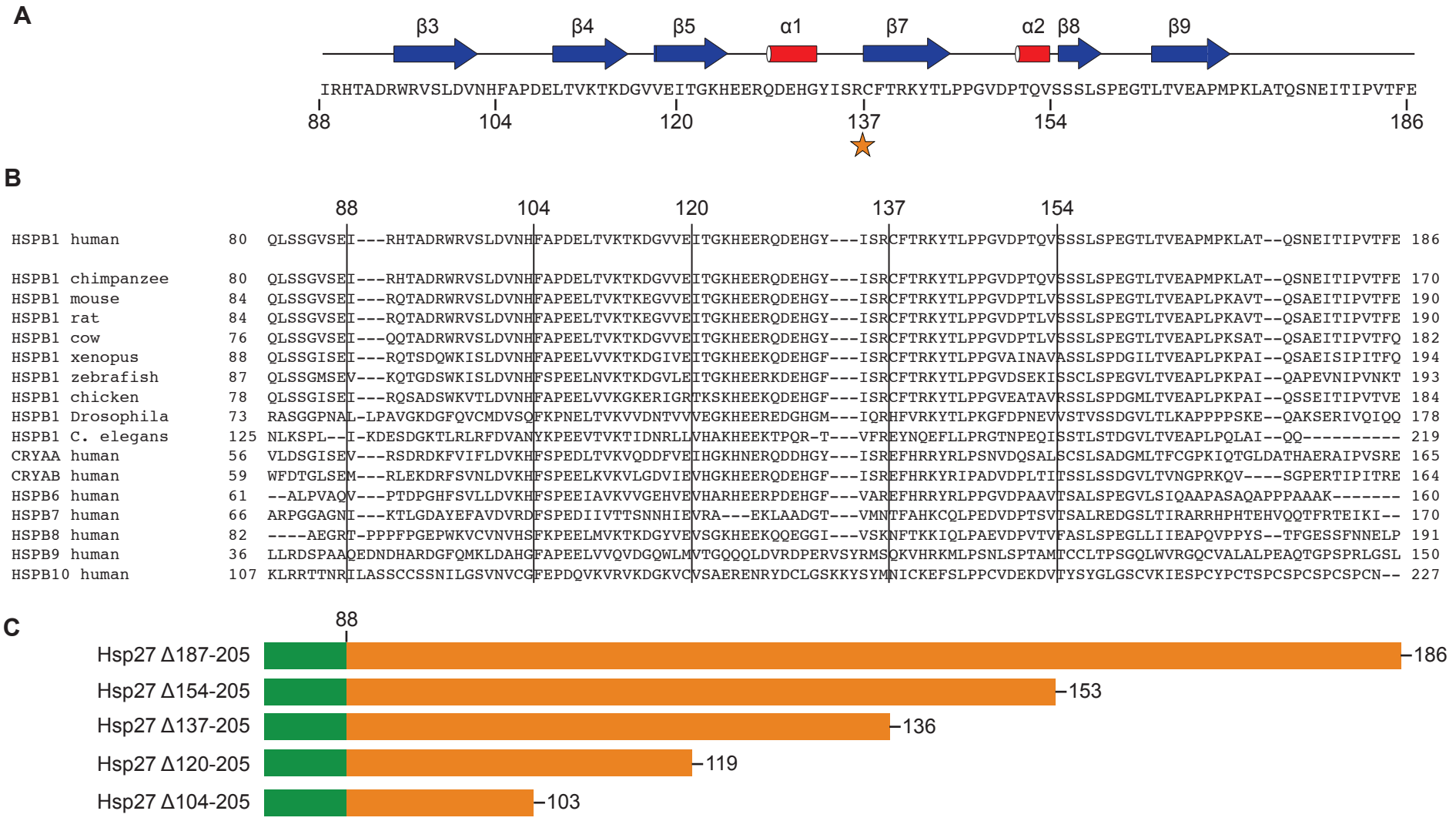

Figure 4. Alignment of human Hsp27 protein sequence to evolutionarily related sHsps. **A:** Schematic representaiton of human Hsp27 α-crystallin domain secondary structure with the C137 residue important for dimer formation marked by a star. **B:** Sequence alignment of HSPB1 (Hsp27) protein sequence and other related sHsps (CRYAA, CRYAB, HSPB6-10). Vertical lines show the design scheme of Hsp27 nested deletion clones. **C:** Cartoon of Hsp27 nested deletion clones.

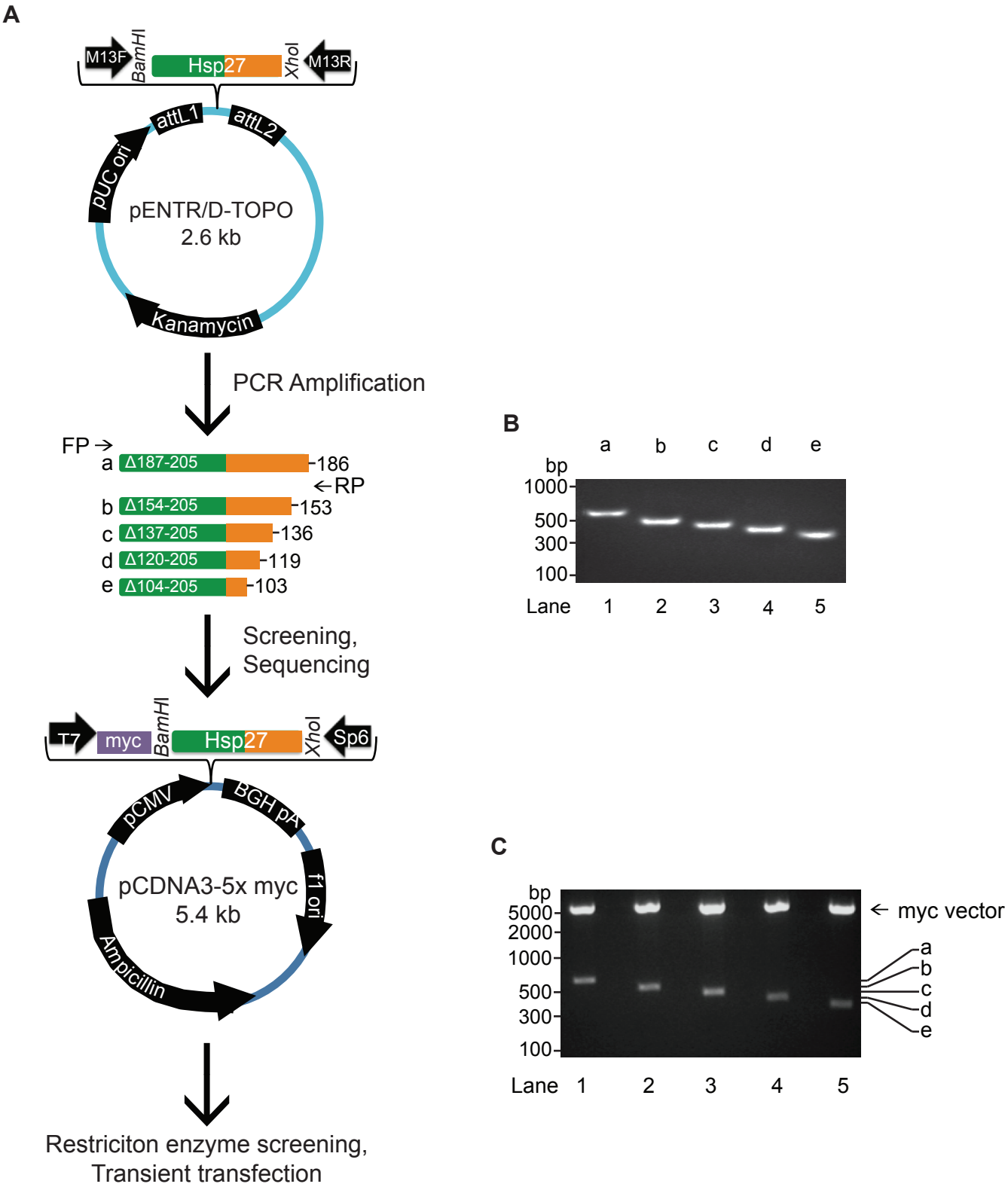

Figure 5. Generation of Hsp27 deletion mutants in mammalian expression vectors. **A:** Hsp27 clones were amplified by PCR with forward (FP) and reverse (RP) primers (Table 2) flanking the regions of interest. Hsp27 DNA inserts (a-e) were ligated into the mammalian expression vector pCDNA3-5 x myc. **B:** Hsp27 deletion PCR products were run on a 1% agarose gel. **C:** Agarose gel restriction enzyme analysis using *BamH*I and *Xho*I to identify myc vectors (5.5 kb) containing the Hsp27 deletion DNA.

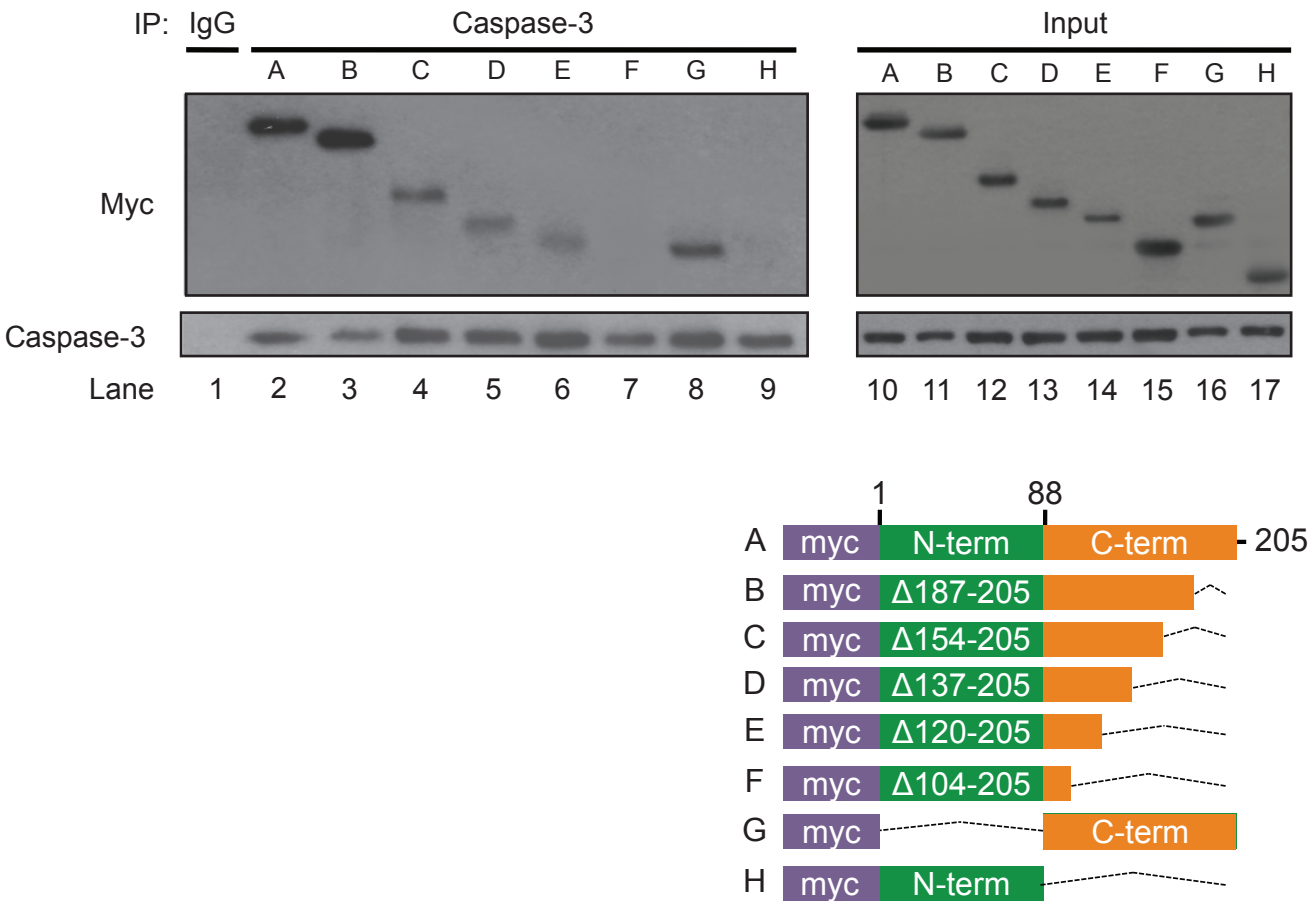

Figure 6. Effect of myc-tagged Hsp27 deletion mutants on the association with caspase-3. Lysates from HeLa cells transiently transfected with Hsp27 clones were immunoprecipitated (IP) using anti-caspase-3 or IgG control antibodies (lane 1). IP and Input were analyzed by immunoblotting with anti-myc and anti-caspase-3 antibodies. The data presented is representative of three independent experiments.

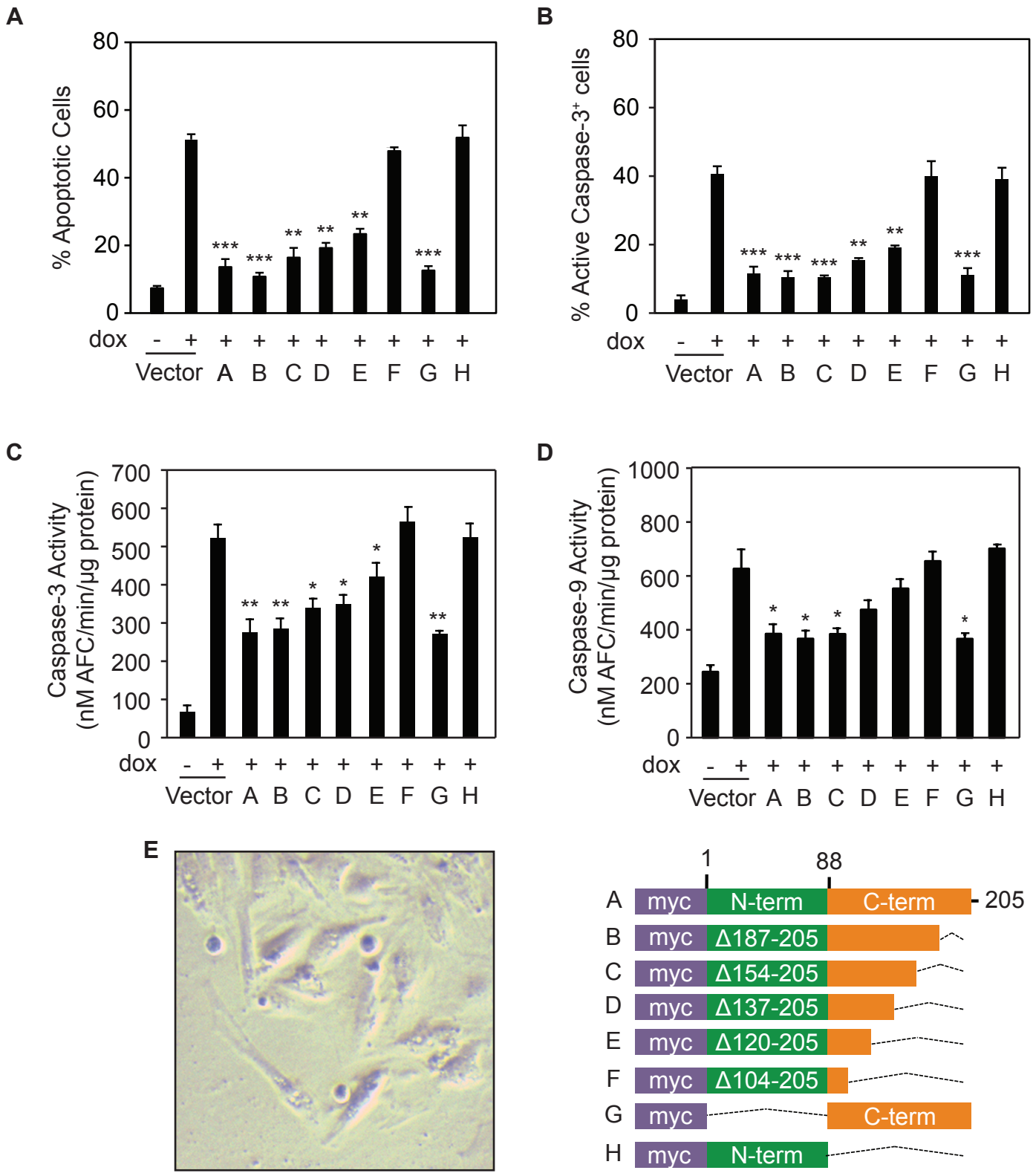

Figure 7. Hsp27 C-terminal deletion clones inhibit caspase activity. H9c2 rat cardiomyocyte cells were transiently transfected with myc-tagged Hsp27 deletion mutants and treated with 10 µM doxorubicin (dox) or DMSO-diluent control (-) for 12 h. **A-B:** Percentage of apoptotic cells and active caspase-3 was determined using Annexin V-APC/7-AAD and anti-active caspase-3-FITC staining, respectively. **C-D:** Caspase-3 and -9 activity was determined using the caspase activity assay and the fluorescent substrate DEVD-AFC and LEHD-AFC, respectively. (* $p<0.05$; ** $p<0.01$; *** $p<0.001$) **E:** Cultured H9c2 cells. Data is expressed as mean of three experiments ± SEM. Flow cytometry analysis performed by Dr. Oliver Voss.

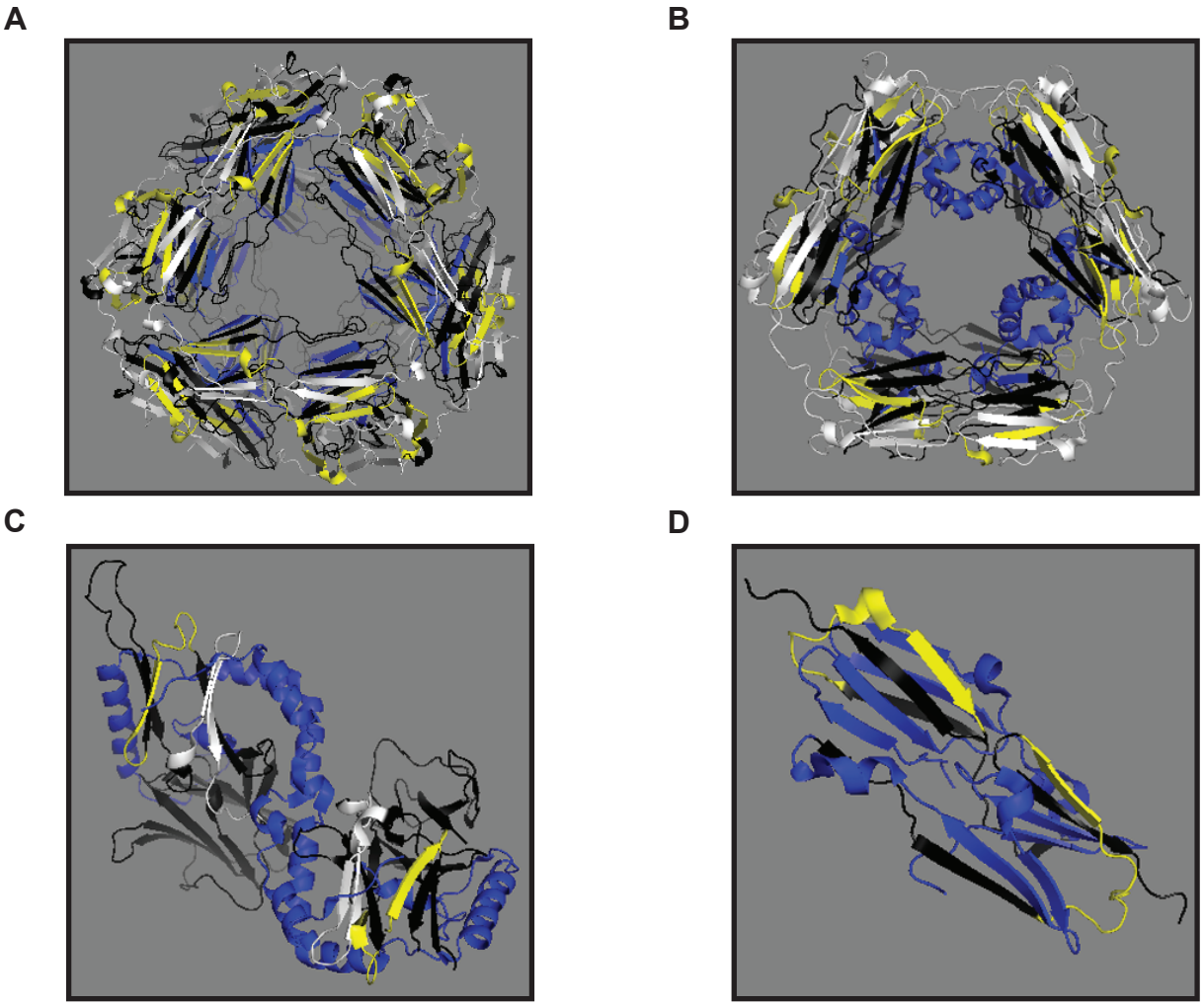

Figure 8. Comparison of completely resolved sHsp crystal structures. The sHsps with completely crystallized oligomeric structures were examined for their ability to serve as a model for the yet unresolved Hsp27 structure. **A:** Structure of *Methanococcus janaschii* (archaean) Hsp16.5, a spherical oligomer made of 24 monomer subunits (91). Hsp16.5 was determined to be the most suitable structural model for Hsp27 based on sequence homology and secondary structure similarity. **B:** Structure of *Triticum aestivum* (wheat) Hsp16.9, composed of two hexameric rings (92). **C:** Structure of *Taenia saginata* (flatworm) Tsp36, a dimer with two α-crystallin domains per subunit (94). **D:** Partial structure of *Xanthomonas axonopodis* (bacteria) sHspA which forms a functional dodecamer (93). (blue = N-terminal; black = C-terminal; yellow = region corresponding to Hsp27 aa 104-119; white = region corresponding to Hsp27 aa 154-186)

A

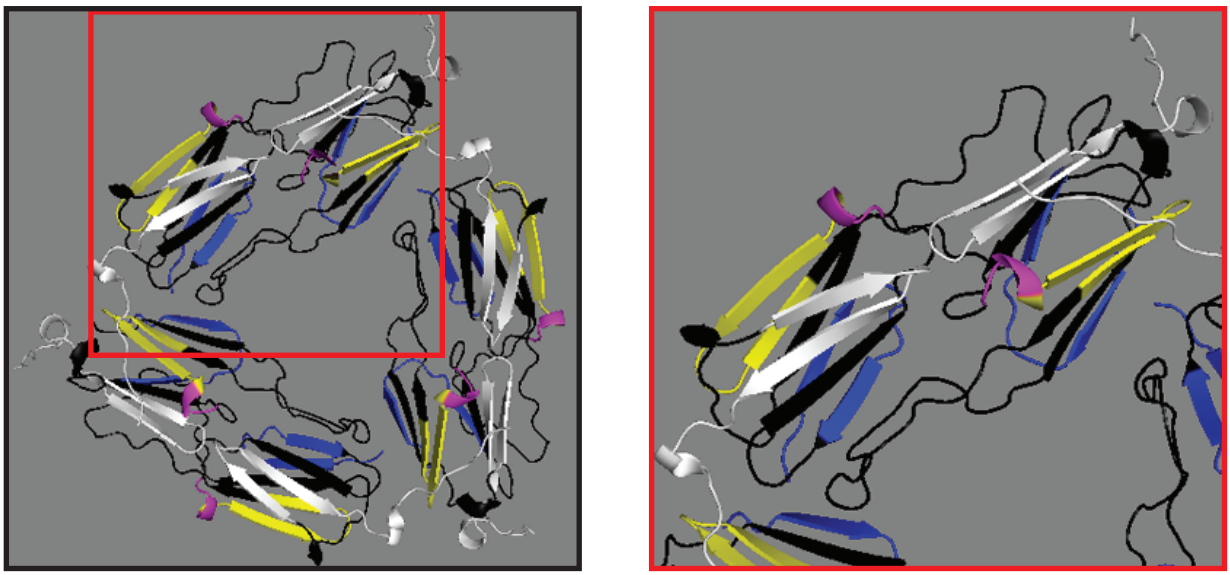

B

Human Hsp27 aa sequence

Amino Acid		Accessibility
88	Glu	<15%
89	Arg	<15%
90	His	<15%
91	Thr	30-45%
92	Ala	45-55%
93	Asp	15-25%
94	Arg	<15%
95	Trp	<15%
96	Arg	<15%
97	Val	<15%
98	Ser	<15%
99	Leu	<15%
100	Asp	<15%
101	Val	<15%
102	Asn	15-25%
103	His	<15%
104	Phe	25-30%
105	Ala	15-25%
106	Pro	30-45%
107	Asp	15-25%
108	Glu	<15%
109	Leu	15-25%
110	Thr	<15%
111	Val	<15%
112	Lys	<15%
113	Thr	<15%
114	Lys	<15%
115	Asp	15-25%
116	Gly	15-25%
117	Val	<15%
118	Val	<15%
119	Glu	<15%
120	Ile	<15%

Human Hsp27 aa sequence

Amino Acid		Accessibility
121	Thr	25-30%
122	Gly	<15%
123	Lys	25-30%
124	His	15-25%
125	Glu	15-25%
126	Glu	55-60%
127	Arg	15-25%
128	Gln	30-45%
129	Asp	60-65%
130	Glu	15-25%
131	His	<15%
132	Gly	25-30%
133	Tyr	25-30%
134	Ile	25-30%
135	Ser	25-30%
136	Arg	25-30%
137	Cys	25-30%
138	Phe	<15%
139	Thr	15-25%
140	Arg	30-45%
141	Lys	30-45%
142	Tyr	30-45%
143	Thr	30-45%
144	Leu	<15%
145	Pro	25-30%
146	Pro	<15%
147	Gly	<15%
148	Val	<15%
149	Asp	25-30%
150	Pro	<15%
151	Thr	25-30%
152	Gln	<15%
153	Val	15-25%

Human Hsp27 aa sequence

Amino Acid		Accessibility
154	Ser	<15%
155	Ser	15-25%
156	Ser	<15%
157	Leu	30-45%
158	Ser	30-45%
159	Pro	<15%
160	Glu	15-25%
161	Gly	<15%
162	Thr	30-45%
163	Leu	<15%
164	Thr	30-45%
165	Val	15-25%
166	Glu	<15%
167	Ala	<15%
168	Pro	<15%
169	Met	<15%
170	Pro	<15%
171	Lys	15-25%
172	Leu	<15%
173	Ala	<15%
174	Thr	<15%
175	Gln	<15%
176	Ser	30-45%
177	Asn	30-45%
178	Glu	<15%
179	Ile	<15%
180	Thr	15-25%
181	Ile	30-45%
182	Pro	30-45%
183	Val	<15%
184	Thr	45-55%
185	Phe	<15%
186	Glu	45-55%

Figure 9. Hsp16.5 can serve as a structural model for Hsp27. A: Human Hsp27 modeled after archaean Hsp16.5 crystal structure with zoomed view and potential interaction loops (aa 104-106) highlighted in purple. **B:** Accessibility of Hsp27 model aa calculated by Deep View program to determine regions available for protein-protein interactions. (blue = N-terminal; black = C-terminal; yellow = first potential caspase-3 binding domain (aa 104-120); purple = most accessible aa within binding domain, aa 104-106; white = second potential caspase-3 binding domain (aa 154-186))

Chapter 4

Apigenin Sensitization of NSCLC to Chemotherapy

4.1 Introduction

Non-small cell lung carcinomas (NSCLC) are some of the most common and deadliest types of cancers in the United States. The three NSCLC subtypes, adenocarcinomas (ACC), squamous cell carcinomas (SCC), and large cell carcinomas (LCC), are often found at the advanced stage when the cancer has metastasized to other organs and treatment options are limited and ineffective. The tumor necrosis factor-related apoptosis-inducing ligand (TRAIL) has emerged as a promising anti-cancer drug due to its ability to selectively induce apoptosis via the death receptors (DR) 4 and 5 in various malignancies, including cervical and lung cancers and leukemia, while leaving normal cells unaffected (97-99). TRAIL induces cell death via the extrinsic pathway by binding to DR4 or DR5 resulting in the formation of the DISC complex and subsequent caspase-8 activation (19). Normal cells express low levels of DR4 and DR5, but high levels of decoy receptor 1 and 2 (DcR1 and DcR2), which are structurally similar to DR4 and DR5, but lack an intracellular death domain to transmit the apoptotic signal (100). Through a mechanism that is not well understood, transformed cells express more DR4 and DR5 and less DcR1 and DcR2, thus accounting for the TRAIL sensitivity of many colon, breast, kidney, skin, prostate, and ovarian cancers (98-100). However, not all transformed cells switch from decoy receptor to death receptor expression, and as a result, some cancers have been found to be resistant to TRAIL (100). In addition, Hsp70 has been shown to bind to the intracellular domain of DR5 thereby preventing the formation of the DISC complex and

activation of caspase-8, providing an additional mechanism that mediates TRAIL resistance (101). Although TRAIL is not yet FDA-approved, its clinical relevance was recently assessed in a Phase II clinical trial (data not yet published; http://clinicaltrials.gov/ct2/show/record/NCT00508625). Some adverse side effects have been observed in TRAIL-resistant cells including the promotion of tumor cell invasion in pancreatic ductal adenocarcinoma and colorectal cancer models, suggesting that TRAIL has a pro-tumorigenic role in resistant cancer cells (102,103). Approximately 50% of NSCLC are resistant to TRAIL unless given in combination with various other agents that can sensitize the cells to TRAIL treatment, with no particular bias for one NSCLC subtype (104). Therefore, recent interest has been focused on identifying novel therapeutics that can aid in the sensitization of NSCLC to TRAIL treatment by decreasing or inactivating anti-apoptotic proteins while simultaneously up-regulating or activating pro-apoptotic molecules.

Flavonoids induce changes in signal transduction pathways related to apoptosis by promoting the inactivation of the survival kinase, Akt (also known as Protein kinase B), activation of caspase-3, up-regulation of DRs, and decreased expression of anti-apoptotic proteins including XIAP and sHsps such as Hsp27 (48,61,105-107). Some flavonoids have been shown to induce apoptosis in the absence of a chemotherapeutic drug, like the flavones luteolin (Fig. 1C) in NSCLC and apigenin (Fig. 1B) in leukemia (61,108). Other studies have shown that luteolin and the flavonols quercetin (Fig. 1D) and kaempferol (Fig. 1E) improve the effectiveness of chemotherapy drugs like doxorubicin (dox) or cisplatin to induce apoptosis in resistant pancreatic, prostate, and breast cancers as well as NSCLC (105-107). In addition, cervical cancer cells are sensitized to TRAIL treatment by flavone,

apigenin, and the isoflavone genistein (Fig. 1F) through an undetermined mechanism (109).

In some cases, flavonoid-induced sensitization to chemotherapy drugs has been shown to be caused by their effects on proteins involved in apoptosis (53,59,60). Hsp27 expression was found to be upregulated in numerous cancers, including breast, endometrial, lung, and prostate cancers, and it is commonly used as a prognostic marker (110). Importantly, the down-regulation of Hsp27 expression by siRNA sensitized the NSCLC cell line A549 to TRAIL-induced apoptosis (83). The flavonoids quercetin, kaempferol, and luteolin are all able to reduce Hsp27 expression via an undetermined mechanism that involves the downregulation of Hsp27 mRNA (111-113). Quercetin, genistein, and kaempferol further increase the level of apoptosis via the up-regulation of Bax, the down-regulation of Bcl-X_L, Bcl-2, and XIAP, and increased cytosolic cytochrome C in leukemia and lung, prostate, pancreatic, and breast cancers (105,106,114). Another important molecule regulated by flavonoids is the TRAIL receptor DR5, which has been shown to contribute more to apoptotic signaling than DR4 (115). DR5 expression increases with quercetin or naringenin (Fig. 1G) treatment in lung cancers and apigenin treatment in leukemia, prostate cancer, and colon cancer, thereby conferring greater sensitivity to TRAIL treatment (116-118). However, the ability of apigenin to sensitize NSCLC to TRAIL-induced apoptosis and the mechanism by which this may occur has not been studied.

In this study, the efficacy of the flavone apigenin to sensitize NSCLC cell lines to TRAIL-induced apoptosis was assessed and the mechanism by which the sensitization occurs was identified. For this purpose, four cell lines were utilized that were

representative of the types and stages of NSCLC, which included A549 (ACC, Stage I), H2009 (ACC, Stage IV), Calu-1 (SCC), and H1299 (LCC). Our findings showed that apigenin and TRAIL function in a synergistic manner to promote caspase-3 dependent apoptosis in all four NSCLC cell lines. We further identified novel aspects in the mechanism responsible for apigenin sensitization, which involved the down-regulation of the anti-apoptotic proteins XIAP and Hsp27, up-regulation of DR5, and disruption of the interaction between Hsp70 and DR5. Collectively, these findings support a model in which apigenin modulates the function of pro- and anti-apoptotic molecules at multiple cellular checkpoints to promote TRAIL-induced apoptosis in NSCLCs.

4.2 Apigenin and TRAIL Act Synergistically to Induce Apoptosis in NSCLC

In order to determine the effect of apigenin and TRAIL combination treatments on NSCLC cells, four cell lines were utilized that represent the three subtypes of NSCLC at various stages, which included A549 (ACC, Stage I), H2009 (ACC, Stage IV), Calu-1 (SCC), and H1299 (LCC). The effect of combination treatments was assessed by measuring cell viability using the MTT assay. Cells were treated with 1, 10, 25, and 50 μM apigenin or DMSO-diluent control for 24 h prior to the addition of 25, 50, and 100 ng/ml TRAIL or TRAIL-buffer control for an additional 24 h. In A549 cells, treatments with the DMSO-diluent control, 1, or 10 μM apigenin had no effect on cell viability at any concentration of TRAIL tested (Fig. 10A, diamonds, squares, and triangles). However, in the presence of 25 μM apigenin, 50% of cells lost viability when in combination with 100 ng/ml TRAIL (Fig. 10A, circles). In the presence of 50 μM apigenin, only 40% of cells were viable at all concentrations of TRAIL tested (Fig. 10A, inverted triangles). Similar to A549 cells, H2009

cells were unaffected by 1 and 10 μM apigenin treatments (Fig. 10A, squares and triangles). The addition of either 25 or 50 μM apigenin alone resulted in a 40% loss in cell viability, while the combination treatments of 25 or 50 μM apigenin with 100 ng/ml TRAIL caused a further loss of 80% in cell viability (Fig. 10A, circles and inverted triangles). Calu-1 and H1299 cells responded to combination treatments similarly, with less than 10% loss in cell viability observed for 1 μM apigenin treatments at all concentrations of TRAIL tested (Fig. 10A, squares). Calu-1 cells showed 60% cell viability with 10 and 25 μM apigenin treatment when combined with 100 ng/ml TRAIL (Fig. 10A, triangles and circles), which decreased to 25% cell viability with 50 μM apigenin treatment at all concentrations of TRAIL tested (Fig. 10A, inverted triangles). Similar to H2009 cells, H1299 cells showed a sensitivity to 10, 25, and 50 μM apigenin treatment that when combined with 100 ng/ml TRAIL resulted in 50%, 40%, and 20% cell viability, respectively (Fig. 10A, triangles, circles, and inverted triangles). Our data showed that 25 and 50 μM apigenin cause a significant (p<0.0001) loss in cell viability in all cell lines as compared to no apigenin treatment (Fig. 10A, circles and inverted triangles). In addition, the 10 μM apigenin treatment induced significantly lower cell viability in Calu-1 (p<0.0001) and H1299 (p<0.01) cells (Fig. 10A, triangles). These results suggest that apigenin and TRAIL combination treatments are able to reduce cell viability significantly more than either treatment alone.

To determine whether the observed effect of combination treatment on cell viability is the result of an additive, synergistic, or antagonistic drug effect, isobolograms were generated (Fig. 10B). The IC_{50} of apigenin treatment alone and TRAIL treatment alone was used to construct the line of additivity for the isobologram of each cell line, and the

combination index (CI) was calculated using the formula described in section 2.12 (Table 4). The combination treatment for all cell lines was found to have a CI < 1, suggesting that apigenin and TRAIL function synergistically, meaning the effects of TRAIL are enhanced by apigenin treatment. A lower CI, such as 0.173 calculated for H2009, may indicate more synergism than the A549 CI of 0.557, but given that the calculated CI is based on estimations (IC_{50}), the error and significance of each CI cannot be determined.

Table 4. Calculated IC_{50} and Combination Index

Cell Line	A_{50} (μM)	T_{50} (ng/ml)	C_{50} (μM)	CI
A549	60.55	1.87×10^{14}	33.74	0.557
H2009	129.52	1631.00	14.47	0.173
Calu-1	172.88	8856.00	22.72	0.131
H1299	169.82	1.95×10^{11}	10.00	0.059

A_{50} = IC_{50} of apigenin alone, T_{50} = IC_{50} of TRAIL alone, C_{50} = IC_{50} of apigenin when combined with 100 ng/ml TRAIL, CI = combination index

Further characterization of the apigenin and TRAIL combination treated NSCLC cells was done by analyzing the contribution of apoptosis to the observed decreased cell viability. For this purpose, cells were treated with two concentrations of apigenin. A549 and Calu-1 cells were treated with 25 and 50 μM apigenin, while H2009 and H1299 cells were treated with 10 and 25 μM apigenin for 18 h followed by an additional 6 h with 25, 50, or 100 ng/ml TRAIL. Apoptosis was evaluated by staining with Annexin V-APC/7-AAD and anti-active caspase-3-FITC. In all cell lines, DMSO-diluent control-treated cells exhibited apoptosis and active caspase-3 in less than 8% of cells [Fig. 11A and B, TRAIL (-)/Apigenin (-)]. Apigenin and TRAIL treatment alone showed 7-12% apoptotic and active caspase-3 cells, which was not found to be statistically significant when compared to the DMSO-control [Fig. 11A and B, TRAIL (-)/Apigenin (25 or 50) and TRAIL (100)/Apigenin (-

)]. Combination treatments increased apoptosis and active caspase-3 ranging from 15% for the lowest concentrations of apigenin and TRAIL to 37% for the highest concentrations (Fig. 11A and B). In A549 cells, combination treatments with 25 μM apigenin resulted in apoptosis in about 20% of cells, while 50 μM apigenin induced 30% apoptosis in all concentrations of TRAIL used (Fig. 11A). H1299 cells showed a response similar to A549 cells with combination treatments (Fig. 11A). In H2009 and Calu-1 cells, the percentage of apoptotic cells gradually increased with increasing TRAIL concentration for each apigenin concentration (Fig. 11A). However, in all cell lines, samples treated with the same concentration of apigenin were not found to have a statistically significant increase in apoptotic cells when treated with different concentrations of TRAIL. Staining for active caspase-3 in A549 cells after 25 μM apigenin and 25 ng/ml TRAIL treatment showed 10% positive cells, which increased to about 20% with 50 ng/ml TRAIL or 100 ng/ml TRAIL treatment (Fig. 11B). Increasing TRAIL concentration in combination with 50 μM apigenin gradually increased the percentage of active caspase-3^+ cells from 29% to 34% in A549 cells (Fig. 11B). Calu-1 cells also showed a gradual increase in active caspase-3 with increasing TRAIL and apigenin concentration (Fig. 11B). Both H2009 and H1299 cells showed 15-20% active caspase-3^+ cells when treated with 10 μM apigenin and about 30% active caspase-3^+ cells with 25 μM apigenin (Fig. 11B). However, in all cell lines, samples treated with the same concentration of apigenin were not found to have a statistically significant increase in active caspase-3^+ cells when treated with different concentrations of TRAIL. The two concentrations of apigenin used in each cell line showed a significant difference in the percentage of apoptotic and active caspase-3^+ cells (Fig. 11, bracketed

groups, **** $p<0.0001$, *** $p<0.001$). These results show that apigenin and TRAIL combination treatments induce caspase-3-dependent apoptosis in NSCLC.

The specific apoptotic pathway (intrinsic or extrinsic) involved in the promotion of apoptosis by apigenin and TRAIL treatments was determined by caspase activity assays. NSCLC cells were treated with apigenin for 18 h (25 and 50 μM for A549 and Calu-1, 10 and 25 μM for H2009 and H1299) prior to the addition of 25, 50, or 100 ng/ml TRAIL for 6 h. The activity of caspase-3 and -8 was determined using the DEVD-AFC and IETD-AFC assays, respectively (Fig. 12). In A549 cells, control, apigenin alone, or TRAIL alone all showed very little caspase-3 activity, and individual treatments were not statistically significant, which was also shown in H2009 and Calu-1 cells (Fig. 12A). Treatment with 25 μM apigenin increased caspase-3 activity when combined with TRAIL, with 50 and 100 ng/ml TRAIL showing a similar activity level at 50 nM AFC/min/mg protein compared to 30 nM AFC/min/mg protein with 25 ng/ml TRAIL (Fig. 12A). Caspase-3 activity increased with 50 μM apigenin to 60 nM AFC/min/mg protein when combined with 25 ng/ml TRAIL and 75 nM AFC/min/mg protein with 50 and 100 ng/ml TRAIL (Fig. 12A). H1299 cells followed a similar profile of increasing caspase-3 activity with increasing apigenin and TRAIL concentration, with the exception that treatment with TRAIL alone induced significantly higher caspase-3 activity ($p<0.0001$) compared to the control sample (Fig. 12A). H2009 cells showed low levels of caspase-3 activity when treated with 10 μM apigenin combined with 25 or 50 ng/ml TRAIL (10 nM AFC/min/mg protein) that was dramatically increased with 100 ng/ml TRAIL (80 nM AFC/min/mg protein), though still not calculated to be statistically significant (Fig. 12A). Furthermore, H2009 treated with 25 μM apigenin in combination with 25 or 50 ng/ml TRAIL also showed lower caspase-3

activity (75 nM AFC/min/mg protein) as compared to combination treatment with 100 ng/ml TRAIL (160 nM AFC/min/mg protein) (Fig. 12A). Calu-1 cells showed caspase-3 activity of about 170 nM AFC/min/mg protein for all combination treatments of apigenin and TRAIL tested (Fig. 12A). With the exception of Calu-1 cells, all cell lines showed that increasing apigenin treatment resulted in significantly higher caspase-3 activity across the range of TRAIL concentrations tested (Fig. 12A, bracketed groups, * $p<0.05$, *** $p<0.001$, **** $p<0.0001$). However, in all cell lines, samples treated with the same concentration of apigenin were not found to have a statistically significant increase in caspase-3 activity when treated with different concentrations of TRAIL. In parallel, the activity of caspase-8 was assessed in H1299 cells, and treatment with 25 μM apigenin, 100 ng/ml TRAIL, or a combination of 10 μM apigenin and 100 ng/ml TRAIL showed no significant increase in caspase-8 activity as compared to the DMSO-control (Fig. 12B). Treatment with 25 μM apigenin and 100 ng/ml TRAIL did significantly increase caspase-8 activity (Fig. 12B, * $p<0.05$), suggesting that apigenin and TRAIL combination treatment-induced apoptosis occurs via the extrinsic pathway.

4.3 Mechanism of Apigenin Sensitization of NSCLC Cells to TRAIL Treatment

In order to investigate the molecular mechanisms by which apigenin sensitizes NSCLC cells to TRAIL treatment, the expression of apoptotic proteins was assessed by western blots. For this purpose, NSCLC cells were treated with apigenin for 18 h (25 and 50 μM for A549 and Calu-1, 10 and 25 μM for H2009 and H1299) prior to the addition of 100 ng/ml TRAIL for 6 h. Immunoblot of A549 lysates showed that XIAP expression decreases by 40% with apigenin treatment compared to the DMSO-control or TRAIL alone

treated cells (Fig.13A, lanes 1-3). Combination treatments of apigenin and TRAIL decreased XIAP expression to similar levels found in apigenin alone treated cells (Fig. 13A, lanes 4-5 vs. 2). Like A549 cells, H2009 XIAP expression was similar in DMSO-control and TRAIL treated cells, and lower in apigenin and combination treated cells (Fig. 13A, lanes 6-10). In Calu-1 cells, expression of XIAP decreased by 45% with apigenin treatment as compared to the control, increased by about twofold with TRAIL treatment, and then decreased again with the combination treatments (Fig. 13A, lanes 11-15). However, while both 25 and 50 μM apigenin decreased XIAP expression compared to the control in A549 when combined with 100 ng/ml TRAIL, only the 50 μM apigenin and 100 ng/ml treated Calu-1 cells showed lower XIAP expression (Fig. 13A, lanes 4, 5, 14, 15). H1299 cells showed a decrease in XIAP expression with apigenin treatment, no change with TRAIL treatment, and a decrease with combination treatments that was dependent on the apigenin concentration (Fig. 13A, lanes 16-20). The expression of Hsp27 decreased with apigenin treatment and was unaffected by TRAIL treatment in all cell lines compared to the DMSO-control (Fig. 13A, lanes 1-3, 6-8, 11-13, 16-18). In addition, all cell lines showed an apigenin concentration-dependent decrease in Hsp27 expression with combination treatments (Fig. 13A, lanes 4, 5, 9, 10, 14, 15, 19, 20). The expression of BID, a member of the Bcl-2 family and a caspase-8 substrate, was unchanged in samples treated with apigenin alone compared to the DMSO-control in all cell lines (Fig. 13A, lanes 1, 2, 6, 7, 11, 12, 16, 17). However, in the presence of TRAIL, A549 and Calu-1 cells showed no changes in BID expression compared with the control, while H2009 and H1299 showed about a 50% decrease of BID as compared to the control (Fig. 13A, lanes 3, 8, 13, 18). Apigenin and TRAIL combination treatments greatly reduced the prevalence of BID in all cell lines, from

45 % in Calu-1 cells treated with 50 μM apigenin and 100 ng/ml TRAIL to 98% in H1299 cells treated with 25 μM apigenin and 100 ng/ml TRAIL, suggesting the proteolytic processing of BID to *t*-BID by caspase-8 (Fig. 13A, lanes 4, 5, 9, 10, 14, 15, 19, 20).

Apigenin increased the expression of DR5 in A549 cells in a concentration-dependent manner as compared to the DMSO-control (Fig. 13A, lanes 2, 4, 5 vs. lane 1). In addition, TRAIL treatment had no effect on the expression of DR5 (Fig. 13A, lane 3). A similar effect of apigenin and TRAIL treatments was observed in H2009, Calu-1, and H1299 cells as well (Fig. 13A, lanes 6-20). Interestingly, other Hsps, including the DR5 chaperone Hsp70, were not effected by apigenin or the combination treatment of apigenin and TRAIL, unlike Hsp27. (Fig. 13A, lanes 2, 4, 5, 7, 9, 10 12, 14, 15, 17, 19, 20). These results show that TRAIL sensitization by apigenin includes the down-regulation of anti-apoptotic proteins as well as the up-regulation of the TRAIL receptor, DR5.

It was previously reported that Hsp70 associates with the intracellular death domain of DR5, thereby blocking DR5 signaling and preventing the activation of the apoptotic casacade (101). Moreover, silencing of Hsp70 sensitized cells to drug-induced apoptosis by allowing DISC formation on the DR5 receptor (119). Based on these findings, it was hypothesized that apigenin sensitizes NSCLC cells to TRAIL by disrupting the Hsp70-DR5 complex. To test this hypothesis, A549 and H1299 cells were selected since they showed the greatest decrease in BID levels with apigenin-TRAIL combination treatments (Fig. 13A, lanes 4, 5, 19, 20). Cell lysates from A549 and H1299 cells treated with apigenin (50 μM for A549 or 25 μM for H1299) for 18 h followed by 100 ng/ml TRAIL for an additional 6 h and were immunoprecipitated with anti-DR5 or IgG isotype control antibodies, resolved by SDS-PAGE, and immunoblotted with anti-Hsp70 and anti-DR5

antibodies (Fig. 13B and Table 3). The results showed that TRAIL treatment alone does not affect the Hsp70-DR5 interaction in A549 cells, while it enhances Hsp70 binding to DR5 by 50% compared to the control in H1299 cells (Fig. 13B, lane 2 vs. 4). Apigenin treatment alone decreases Hsp70 association to DR5 by more than 70% compared to the control in both cell lines (Fig. 13B, lane 3). However, a repeat of this experiment showed that apigenin alone reduced Hsp70 binding by 25%, so while it is clear that apigenin is able to disrupt the Hsp70-DR5 complex, the extent to which this occurs will require further investigation (data not shown). Regardless, the apigenin and TRAIL combination treatment resulted in a loss of more than 80% of Hsp70 binding to DR5 in all repeats (Fig. 13B, lane 5). Taking the previous results into consideration, the data suggest that apigenin and TRAIL combination treatments not only increase DR5 expression, but also disrupt the Hsp70-DR5 complex thereby freeing the DR5 intracellular death domain for DISC formation and promoting the activation of caspase-8, as shown in Fig. 12B.

4.4 Conclusion

In this project the ability of the flavone apigenin to sensitize NSCLC cells to TRAIL treatment was investigated. Four NSCLC cell lines, A549, H2009, Calu-1, and H1299, were treated with various combinations of apigenin and TRAIL and cell viability, percentage of apoptotic and active caspase-3 cells, and changes in apoptotic protein expression was assessed. Our findings showed that apigenin sensitizes NSCLC to TRAIL-induced caspase-3-dependent apoptosis by increasing the expression of the TRAIL receptor, DR5, and decreasing the expression of anti-apoptotic proteins like Hsp27 and XIAP. In addition, treatment with apigenin decreased the association of Hsp70 with DR5, probably facilitating

the release of DR5 to allow it to transmit the TRAIL-induced death signal into the cell. These results suggest that apigenin functions on multiple levels to effectively sensitize NSCLC cells to TRAIL treatment.

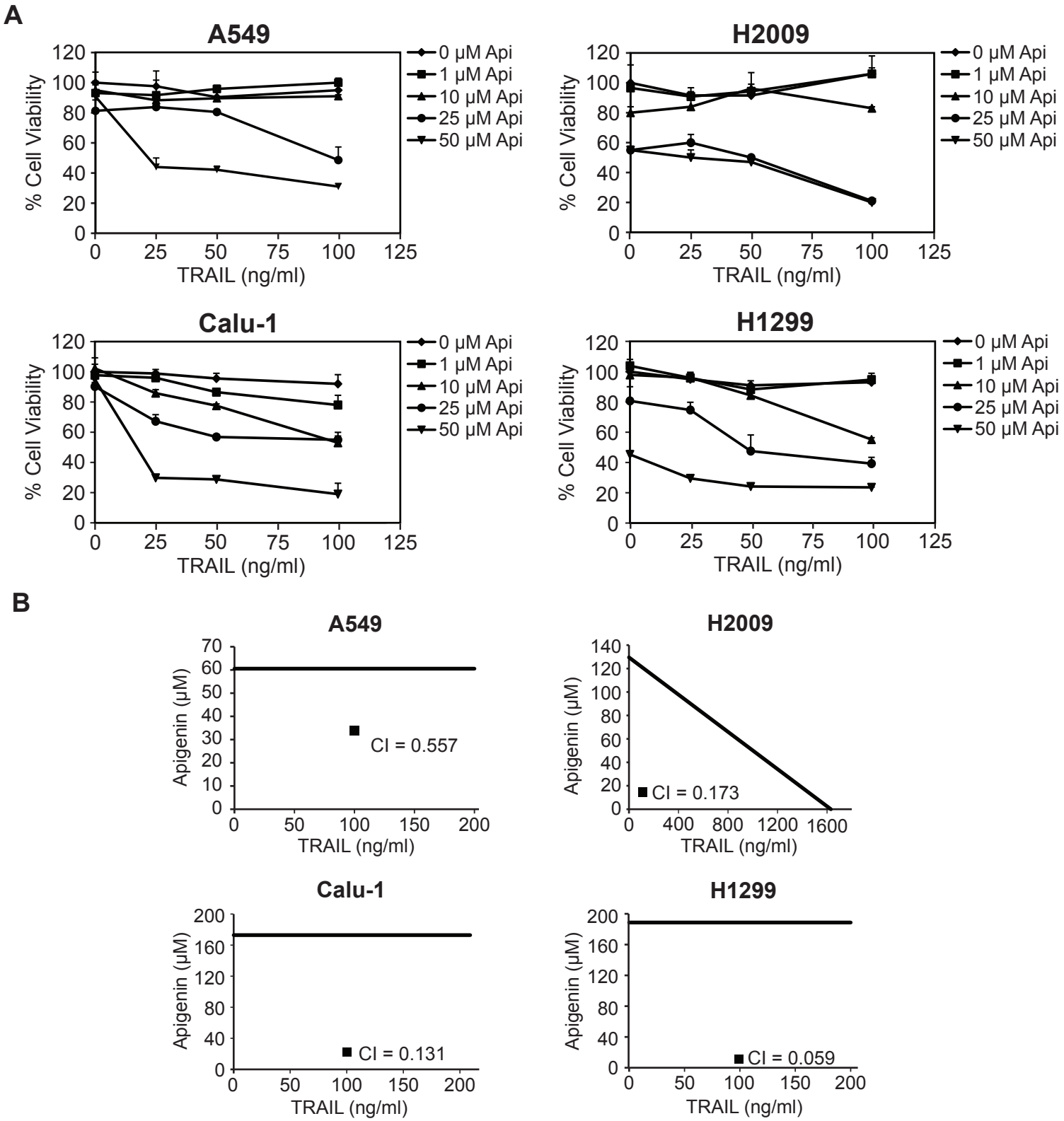

Figure 10. Apigenin sensitizes NSCLC to TRAIL treatment in a synergistic manner. A: Cell viability of NSCLC cells treated with apigenin (Api) for 24 h and TRAIL added for an additional 24 h was determined by MTT assay. The data were analyzed by two-way ANOVA and the 25 and 50 μM Api treatments were found to be statistically significant (p<0.0001) for all cell lines. In addition, statistical significance was also determined for the 10 μM Api treatment of Calu-1 cells (p<0.0001) and the 10 μM Api treatment of H1299 cells (p<0.01). **B:** Isobolograms of combination treatments shown in (A) with calculated combination index (CI <1, synergistic; CI =1, additive; CI >1, antagonistic). Data is expressed as mean of three experiments ± SEM.

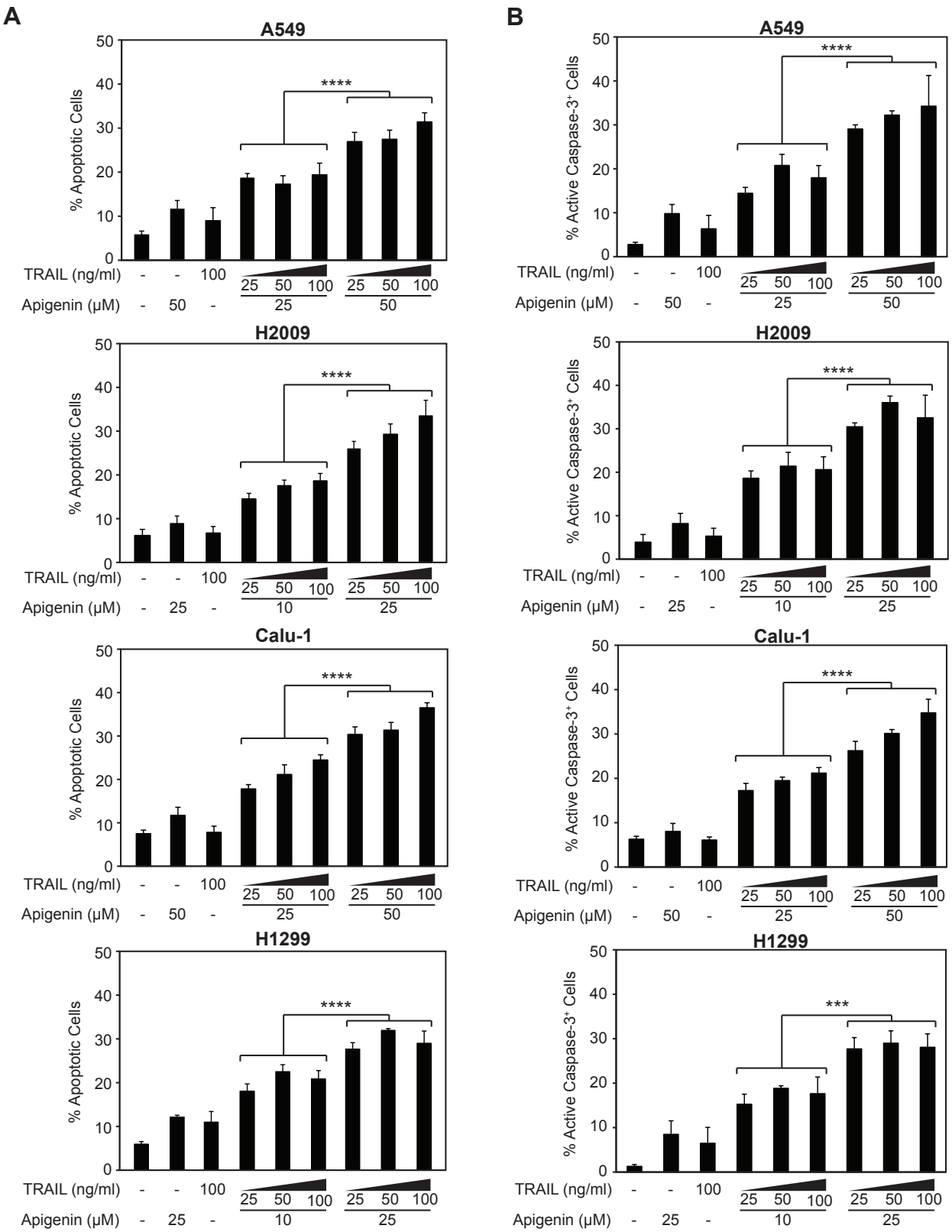

Figure 11. Apigenin and TRAIL combination treatments induce caspase-3 dependent apoptosis. NSCLC cell lines were treated with two concentrations of apigenin (10 and 25 μM for H2009 and H1299; 25 and 50 μM for A549 and Calu-1) or DMSO control (-) for 18 h and 25, 50, or 100 ng/ml TRAIL or TRAIL buffer control (-) was added for an additional 6 h. **A-B:** Percentage of apoptotic cells and active caspase-3 was determined using Annexin V-APC/7-AAD and anti-active caspase-3-FITC staining, respectively. Statistical analysis was done using two-way ANOVA to compare the effect of apigenin concentration across a range of TRAIL concentrations (*** $p<0.001$; **** $p<0.0001$). TRAIL concentration was not found to have a significant effect within each apigenin treatment group. Data is expressed as mean of three experiments ± SEM. Flow cytometry analysis performed by Dr. Oliver Voss.

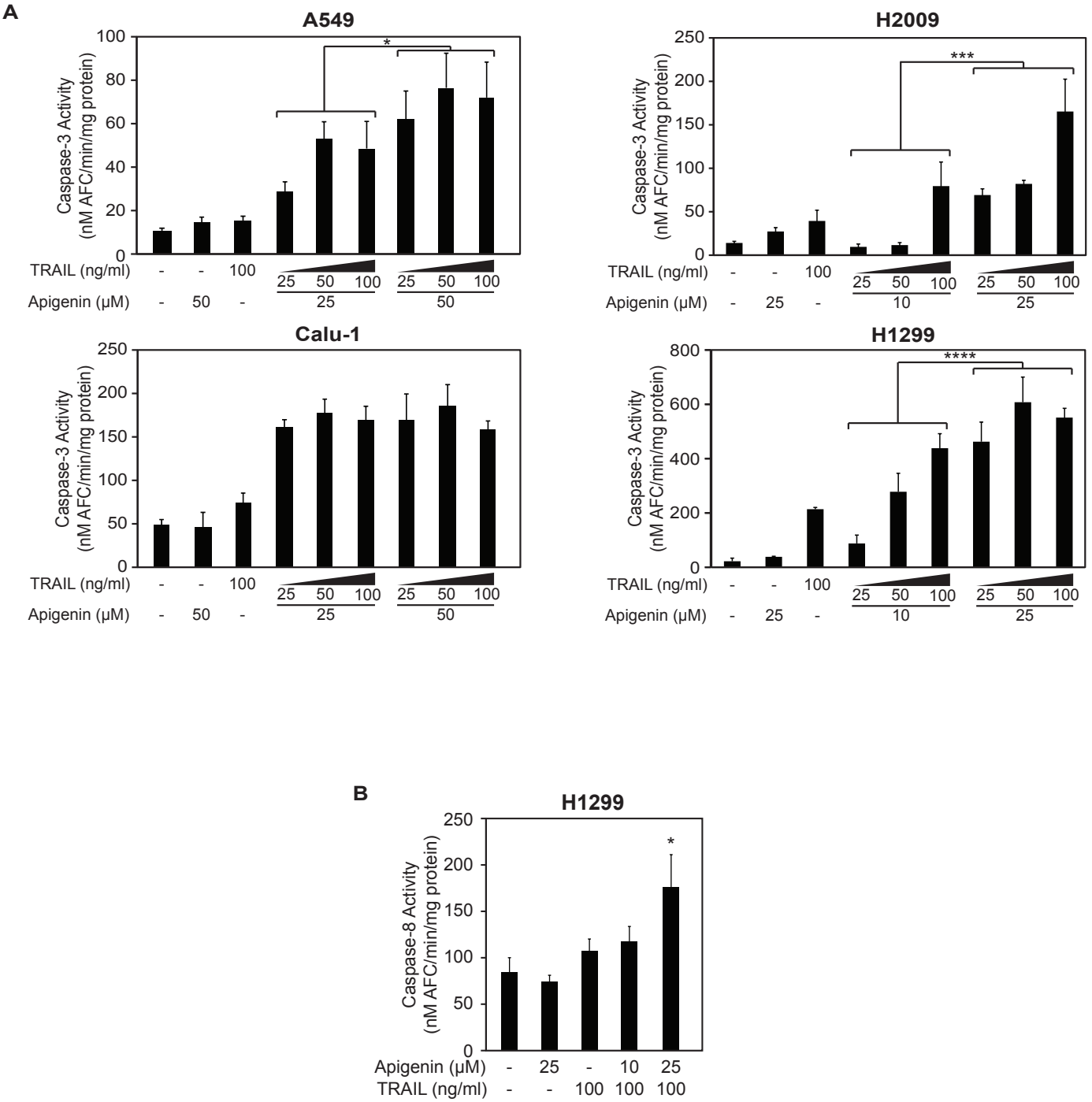

Figure 12. Apigenin and TRAIL combination treatments induce apoptosis via the extrinsic pathway. NSCLC cell lines were treated with two concentrations of apigenin (10 and 25 μM for H2009 and H1299; 25 and 50 μM for A549 and Calu-1) or DMSO-control (-) for 18 h prior to the addition of 25, 50, or 100 ng/ml TRAIL or TRAIL Buffer-control (-) for 6 h. **A-B:** Caspase-3 and -8 activity was determined using the caspase activity assays and the fluorescent substrates DEVD-AFC and IETD-AFC, respectively. Statistical analysis was done using two-way ANOVA to compare the effect of apigenin concentration across a range of TRAIL treatments
(* $p<0.05$; *** $p<0.001$; **** $p<0.0001$). Data is expressed as mean of three experiments ± SEM.

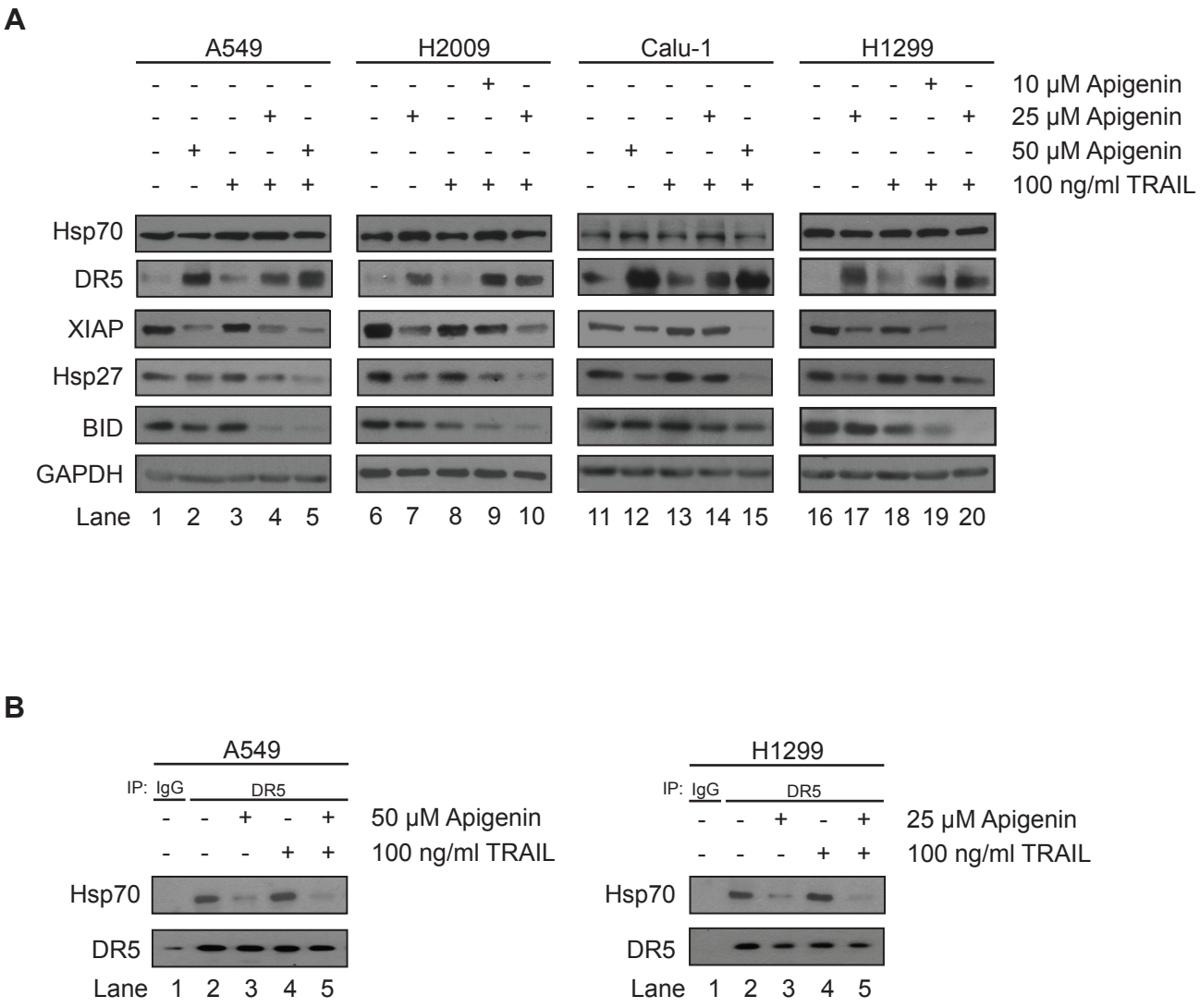

Figure 13. Apigenin sensitizes NSCLC cells to TRAIL treatment via regulation of apoptotic protein expression. NSCLC cells were treated with apigenin for 18 h and TRAIL was added for an additional 6 h. **A:** Cell extracts from treated NSCLC cells were resolved by SDS-PAGE and immunoblotted with anti-Hsp70, anti-DR5, anti-XIAP, anti-Hsp27, and anti-BID. GAPDH was used as a control for equal loading. **B:** A549 and H1299 lysates were immunoprecipitated (IP) using anti-DR5 or IgG control antibodies (lane 1) and samples were analyzed by immunoblotting using anti-DR5 and anti-Hsp70 antibodies. The data presented is representative of two independent experiments. IPs were performed by Dr. Oliver Voss.

Chapter 5

Discussion

It has been well-established that caspase-3 is an essential protease for the execution of apoptosis (12). Numerous proteins ensure the timely induction of apoptosis by tightly regulating the proteolytic activation of caspase-3. The activity of such anti-apoptotic proteins as XIAP, Bcl-2, Bcl-X_L, Hsp70 and Hsp27 prevent apoptosis by inhibiting the pathways that activate caspase-3 (2,28,34). Specifically, our lab has previously shown that Hsp27 is a key apoptotic regulator that binds to caspase-3 to prevent its activation (21).

In this study, we defined the Hsp27 peptide region that is responsible for the inhibition of apoptosis via the specific interaction with caspase-3. First, we showed that the Hsp27 C-terminal is required for the association with caspase-3 and inhibition of its activity, while the N-terminal is unable to bind or inhibit its activity (Fig. 3B-D). Pandey, *et al*. have also shown that Hsp27 associates with caspase-3 (120). However, Bruey, *et al*. were not able to show an interaction between Hsp27 and caspase-3 and suggest an alternative pathway in which Hsp27 anti-apoptotic activity relies on the ability of Hsp27 to bind to cytochrome C, thereby preventing apoptosis upstream of caspase-3 activation (46). Our findings, using purified caspase-3, Hsp27, and active caspase-9 proteins, clearly demonstrated that Hsp27 can bind directly to caspase-3 and cytochrome C is not required for the anti-apoptotic activity of Hsp27 (Fig. 3C and 3D). Indeed, Bruey, *et al*. show that Hsp27 aa 51-88 (within the N-terminal) and Cys137 are required to bind to cytochrome C, suggesting that the Hsp27 C-terminal association with caspase-3 shown here must be cytochrome C-independent (46). It is widely believed that Cys137, the only cysteine

residue in the Hsp27 sequence, is important for a disulfide bridge leading to the dimer formation characteristic of all sHsps (121). As a result, Bruey, *et al*. propose that Hsp27 aa 51-88 bind to cytochrome C, but require an Hsp27 dimer (and by extension, Cys137) for the interaction to occur (46). Our results showed that the Hsp27 C-terminal, which includes Cys137, associates with caspase-3, suggesting that the Hsp27-caspase-3 interaction also requires Hsp27 dimer formation.

After determining that the Hsp27-caspase-3 interaction is mediated solely through the Hsp27 C-terminal, further characterization of this domain was performed to define the specific Hsp27 peptide responsible for binding to caspase-3 using C-terminal nested deletion clones (Fig.5). The results of the IP demonstrated that loss of Hsp27 aa 154-186 causes considerable loss (~50%) of Hsp27 association to caspase-3 (Fig. 6, lane 4). Furthermore, loss of Hsp27 aa 104-119 completely abolished the Hsp27-caspase-3 interaction (Fig. 6, lane 7). These results suggest that Hsp27 may have two caspase-3 specific binding regions, aa 104-119 and aa 154-186. However, our findings cannot distinguish whether both regions contribute equally to the Hsp27-caspsae-3 interaction, or if one region is more important than the other using these clones due to the fact that when aa 104-119 is deleted, aa 154-186 is also deleted. An additional clone that has aa 104-119 deleted but still included aa 154-186 would be required to determine the contribution of each binding region. If each region contributes equally, we would expect to see a 50% reduction in Hsp27 association to caspase-3 following deletion of either region. However, if aa 104-119 is more important binding, we would expect to see a greater loss in the association or even complete abolishment of the Hsp27-caspase-3 complex.

The Hsp27 clones were used to assess if the decreased association of Hsp27 to caspase-3 impaired the ability of Hsp27 to inhibit caspase-3 activation in the H9c2 cardiomyocyte model treated with doxorubicin (Fig. 7). Dox is an effective and commonly used chemotherapeutic drug that induces cardiomyocyte apoptosis as a side effect of cancer treatments (22,76,82). Therefore, the goal of this study was to define the Hsp27 peptide domain that regulates caspase-3 activation. The results of the apoptosis and active caspase-3 staining and caspase-3 activity show that until the loss of aa 104-119, Hsp27 is able to completely inhibit caspase-3 activation and apoptosis (Fig. 7A, B, and C). Theoretically, after the deletion of the peptide region of Hsp27 that is specific for the association with caspase-3, we would expect to see a loss in binding to caspase-3 but not necessarily a loss in the ability of Hsp27 to prevent apoptosis overall, due to the ability of Hsp27 to halt apoptosis upstream of caspase-3 activation. Therefore, the ability of Hsp27 Δ154-205 to inhibit apoptosis (Fig. 7A, clone C) combined with the observed loss of caspase-3 binding of the same clone (Fig. 6, lane 4) suggests that aa 154-186 is a caspase-3 specific binding region. For example, Hsp27 Δ154-205 is likely still able to inhibit apoptosis and caspase-3 activation by binding cytochrome C, for which aa 51-88 and Cys137 are essential, and preventing caspase-9 activation (46). As expected, based on the findings of Bruey, *et al*., Hsp27 Δ137-205 is not able to significantly inhibit caspase-9 activity, probably due to an inability of the Hsp27 clone to bind to cytochrome C (Fig. 7B, clone D). Interestingly, Hsp27 Δ137-205 is still able to inhibit caspase-3 activity and apoptosis, which is suggestive of two important details. First, these results suggest that the Cys137 involved in the oligomerization and dimer formation of Hsp27 is neither required for Hsp27 to associate with caspase-3 (Fig. 6, lane D) nor to inhibit apoptosis and caspase-3

activation (Fig. 7A, clone D). Second, it alludes to the idea that Hsp27 is inhibiting apoptosis downstream of the interaction with cytochrome C and prevention of caspase-9 activation, which therefore must involve caspase-3, the substrate of caspase-9. Altogether, these results support the hypothesis that Hsp27 contains two distinct caspse-3 binding domains that contribute unequally to the protective effect of Hsp27. The first binding region deleted in these experiments, aa 154-186, merely stabilizes and promotes the Hsp27-caspase-3 interaction. The second binding region, aa 104-119, is the most vital and, although Hsp27 Δ120-205 shows considerably less binding to caspase-3 than Hsp27 wt, the presence of aa 104-119 is still able to completely inhibit caspase-3 activation downstream of caspase-9.

With two potential caspase-3 specific binding regions within Hsp27, we further examined the Hsp27 crystal structure with the goal of defining the most accessible aa that would be available for protein-protein interactions. Unfortunately, only the Hsp27 α-crystallin domain was recently elucidated, which is unable to take into consideration the aa accessibility within the full, functional Hsp27 oligomer (95,96). Therefore, other fully crystallized sHsps were examined for their potential to serve as a model for Hsp27 structure, and it was determined that the archaean Hsp16.5 is likely the most structurally similar to Hsp27 (Fig. 8A). Assessment of the aa accessibility of Hsp27 modeled after Hsp16.5 revealed several accessible regions within the two potential caspase-3 binding domains. Based upon our previous results, our analysis was focused on Hsp27 aa 104-119. Only a few residues within this region were found to be more accessible than the surrounding peptide (aa 104-106; Fig. 9B). Interestingly, aa 104-106 corresponded to a loop that rises perpendicularly from the planar surface of the Hsp27 oligomer model,

contributing to the increased accessibility of those particular residues (Fig. 9A). Depending on the accuracy of the Hsp27 model, aa 104-106 could be the residues that directly interact with caspase-3 to inhibit its activity, and further experiments are required to validate this hypothesis.

Following the dissection of the structural role of Hsp27 during its inhibition of caspase-3 activity, we determined the function of Hsp27 and other anti-apoptotic proteins within the context of apoptotic regulation of lung cancer cells. For this purpose, the ability of flavonoids to sensitize the normally chemotherapy-resistant NSCLC cells was assessed. The therapeutic potential of flavonoids has been widely recognized due to their ability to modulate protein expression and activity in numerous diseases including cancer (48). The flavonoid luteolin has been shown to induce apoptosis in A549 cells via the intrinsic pathway by inhibiting NF-κB and downregulating Bcl-2 and Bcl-X_L (108). Other flavonoids, including quercetin and kaempferol, are able to similarly regulate anti-apoptotic proteins such as Bcl-2, though without the addition of a chemotherapeutic drug, they lack the ability to induce apoptosis (105,106). Apigenin has been shown to play both roles with its ability to induce apoptosis independently in leukemia cells and sensitize cervical cancer cells to chemotherapeutic treatment (61,109). The possibility of this dual mechanism of action suggests that different flavonoids will have different effects depending on the cell type being treated.

In this study we examined the effect of apigenin on NSCLC cells. We showed that apigenin, up to 50 μM in A549 and Calu-1 cells and 25 μM in H2009 and H1299 cells, has relatively little effect on cell viability and does not induce apoptosis in four different NSCLC cell lines (Fig. 10A, and 11A). This is in agreement with other findings that show apigenin

does not cause cell death in lung cancer cells at similar concentrations (122,123). Interestingly, others have shown that apigenin concentrations two to four times higher than those used in this study are able to induce apoptosis in A549 cells (123). Also of note, 50 μM apigenin has been shown to induce greater than 50% cell death in leukemia cells and other solid epithelial cancers including prostate, breast, and cervical cancer cells (63,124-126). This suggests that NSCLC cells are uniquely resistant to apigenin-induced apoptosis.

Since apigenin is unable to kill NSCLC cells on its own, we examined other ways in which it may aid in the treatment of lung cancers. As mentioned above, flavonoids have been shown to sensitize cancer cells to chemotherapy drugs like dox and cisplatin (105,106). Specifically, apigenin sensitizes cervical cancer cells to TRAIL treatment (109). This study focused on the chemotherapy drug TRAIL due to its remarkable ability to induce apoptosis in cancerous cells without causing adverse side effects in normal cells (97-99,127). However, our results showed that TRAIL alone is not able to induce apoptosis in NSCLC cells (Fig. 10A and 11A), which is in agreement with others (83,128). Our findings showed that apigenin and TRAIL combination treatments induce significantly more apoptosis in NSCLC cells than TRAIL treatment alone (Fig. 10 and 11). Although apigenin and TRAIL combination treatments have not been studied in NSCLC cells, a similar sensitization effect has been shown in leukemia, hepatocellular carcinoma, melanoma, and prostate, colon, breast, and pancreatic cancers (117,129). Altogether, these results suggest that the ability of apigenin to sensitize cells to TRAIL treatment is not limited to just NSCLC cells, but can be applied to a variety of cancers. In addition, our results show that the concentration of apigenin, not TRAIL, is the more important determinant of the efficacy of

the combination treatment (Fig. 11A). For each cell line, increasing apigenin concentration resulted in significantly more apoptosis, while increasing TRAIL concentration had little effect on the level of apoptosis.

After determining that apigenin is able to sensitize NSCLC cells to TRAIL treatment, we investigated the mechanism by which the sensitization occurs. Previous studies have described sensitization mechanisms involving changes in apoptotic protein expression (105-107,109,114,116-118,128,129). Our results showed that apigenin treatment causes an upregulation of the TRAIL receptor DR5 (Fig. 13A). Horinaka, *et al*. have shown that apigenin induces increased expression of DR5 leading to increased sensitivity of TRAIL treatment (117). Quercetin and the flavonone naringenin were also found to increase DR5 expression in NSCLC for greater sensitivity to TRAIL (116,118). Decreased IAP expression, including XIAP and Survivin, has also been shown to be caused by luteolin, quercetin and genistein in lung cancer cells (106,114,116). Our results show that apigenin also downregulates XIAP expression (Fig. 13A, lanes 2, 7, 12, and 17). As previously mentioned, Hsp27 is another anti-apoptotic protein important for the resistance to chemotherapy drugs (110). Quercetin, kaempferol, and luteolin reduce Hsp27 expression in leukemia, cervical cancer, and lung cancer (111-113). Our results indicate that apigenin is also able to downregulate Hsp27 in NSCLC cells (Fig. 13A, lanes 2, 7, 12, and 17). Together, this data contributes to a mechanism for apigenin sensitization. The increased expression of DR5 would increase the ability of TRAIL to signal the cell to undergo apoptosis, and the decreased expression of Hsp27 and XIAP would further facilitate the activation of the apoptotic signal cascade to activate caspase-3.

Our data showed apigenin increases DR5 expression, though Hsp70 has been shown to bind to the DR5 intracellular death domain thereby preventing formation of the DISC complex and activation of caspase-8 (101). Therefore, we hypothesized that apigenin could promote apoptosis by disrupting the binding of Hsp70 to DR5. Our data showed that apigenin decreases Hsp70 binding to DR5, though the extent to which this occurs requires further investigation, which is enhanced even further when combined with TRAIL treatment (Fig. 13B, lanes 3 and 5). The disruption of Hsp70 binding to DR5 is a novel mechanism for the sensitization of cancer cells by flavonoids. If the increased expression of DR5 is important for the amplification of the TRAIL apoptotic signal, then it can be suggested by corollary that increased availability of the intracellular death domain is equally as integral for chemotherapy sensitivity. This supports the idea that apigenin and TRAIL function synergistically, where apigenin is "priming" the cells for apoptosis without inducing cell death, while TRAIL is the "trigger" that initiates the apoptotic cascade. Apigenin and TRAIL are each unable to kill cells independently since neither the up-regulation of DR5 and liberation of its death domain from Hsp70 caused by apigenin nor TRAIL in the presence of low levels of Hsp70-bound DR5 is sufficient to initiate apoptosis. Both pieces, the priming by apigenin and the addition of TRAIL are required for the successful induction of the apoptotic-signaling cascade.

The goals of this thesis were to define the mechanisms by which proteins inhibit apoptosis. For this purpose, two distinct yet complimentary approaches were taken. First, the specific protein-protein interaction between caspase-3 and Hsp27 was studied to determine the Hsp27 peptide region responsible for associating with caspase-3 to prevent its activation. We discovered that Hsp27 aa 104-119 is essential for the inhibition of

caspase-3, and aa 154-186 likely stabilizes the interaction for efficient Hsp27 binding. Future studies of this association will involve aa substitutions within each binding domain to further define the specific Hsp27 peptide responsible for the inhibition of caspase-3 activity by IP and apoptosis assays. Ideally, these results will lead to a novel therapy utilizing the Hsp27 peptide sufficient to inhibit apoptosis to prevent unwanted cell death, such as the cardiomyocyte apoptosis associated with dox treatment. The second approach to study anti-apoptotic mechanisms used chemotherapy-resistant NSCLC cells. Our data showed that the flavonoid apigenin is able to sensitize NSCLC cells to TRAIL treatment. Furthermore, our results indicate that the downregulation of the anti-apoptotic proteins XIAP and Hsp27, the upregulation of the TRAIL receptor, DR5, and the inhibition of Hsp70 binding to the DR5 death domain are the cause of the sensitization. Future work on this project could involve the further identification of protein expression and/or activity that can account for the sensitization. In addition, the mechanism by which apigenin is able to regulate protein expression can be elucidated by determining the transcription and/or protein degradation pathway(s) affected by apigenin treatment. These findings will hopefully contribute to the development of novel cancer therapies involving the use of natural plant compounds such as apigenin. Therefore, we propose a model to describe the mechanisms of both Hsp27 apoptotic inhibition and apigenin sensitization (Fig. 14).

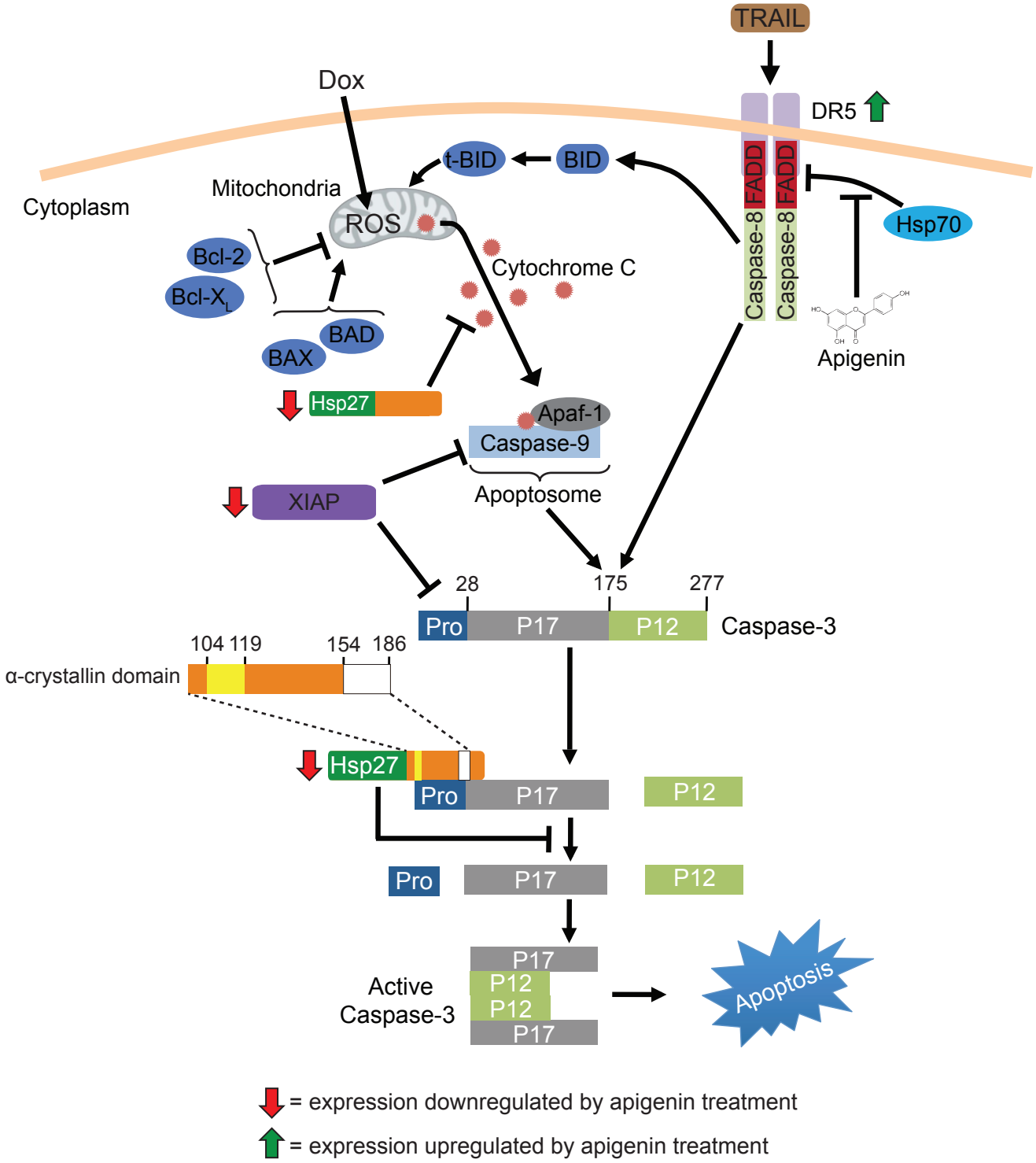

Figure 14. Proposed model for the apigenin sensitization of cancer cells and the structural role of Hsp27 during the inhibition of apoptosis. Apigenin causes the increased expression of the TRAIL receptor DR5 (green arrow) and the decreased expression of the anti-apoptotic XIAP and Hsp27 (red arrow). In addition, apigenin inhibitis the binding of Hsp70 to the intracellular death domain of DR5. Hsp27 inhibits apoptosis by associating with caspase-3. Specifically, Hsp27 aa 104-119 and 154-186 interact with the caspase-3 prodomain to prevent the autocatalytic cleavage necessary for caspase-3 activation.

Acknowledgements

First, I would like to thank Dr. Andrea Doseff for giving me the opportunity to perform research in her lab and for her critical reading of this thesis. I am very grateful and appreciative of the guidance and mentorship she has provided me during my undergraduate career. Second, I would like to thank Dr. Oliver Voss for his contribution to this work and for the many techniques and analytical skills he has patiently taught me over the years. Finally, thank you to all the members of the Doseff lab, past and present. I have learned so much from each of you scientifically, professionally, and culturally, and I will always remember and cherish the time we spent together. My undergraduate years would not have been the same without all of you, and I do not doubt that this experience will continue to shape my life for many years to come.

This research was supported by the Pelotonia Undergraduate Fellowship, the American Heart Association Summer Undergraduate Research Fellowship, and the College of Arts and Sciences Undergraduate Research Scholarship to J.C.T., and the National Science Foundation (NSF) Division of Molecular and Cellular Biosciences (MCB) 0542244 and National Institutes of Health (NIH)/National Heart, Lung, and Blood Institute (NHLBI) R01 HL075040 to A.I.D.

References

1. Kochanek, K. D., Xu, J., Murphy, S. L., Miniño, A. M., and Kung, H. C. (2011) Deaths: final data for 2009. *National Vital Statistics Reports* **60**, 1-116
2. Ciocca, D. R., and Calderwood, S. K. (2005) Heat shock proteins in cancer: diagnostic, prognostic, predictive, and treatment implications. *Cell Stress Chaperones* **10**, 86-103
3. Levine, A. J. (1997) p53, the cellular gatekeeper for growth and division. *Cell* **88**, 323-331
4. Croce, C. M. (2008) Oncogenes and cancer. *N Engl J Med* **358**, 502-511
5. Scaffidi, C., Schmitz, I., Krammer, P. H., and Peter, M. E. (1999) The role of c-FLIP in modulation of CD95-induced apoptosis. *J Biol Chem* **274**, 1541-1548
6. Hong, W. K., and American Association for Cancer Research. (2010) *Holland Frei cancer medicine 8*, 8th ed., People's Medical Pub. House, Shelton, Conn.
7. Jemal, A., Siegel, R., Xu, J., and Ward, E. (2010) Cancer statistics, 2010. *CA Cancer J Clin* **60**, 277-300
8. Horn, L., and Sandler, A. (2010) Angiogenesis inhibitors in lung cancer. in *Lung Cancer: Prevention, Management and Emerging Therapies* (Stewart, D. J. ed., Humana Press, New Jersey
9. Raponi, M., Zhang, Y., Yu, J., Chen, G., Lee, G., Taylor, J. M., Macdonald, J., Thomas, D., Moskaluk, C., Wang, Y., and Beer, D. G. (2006) Gene expression signatures for predicting prognosis of squamous cell and adenocarcinomas of the lung. *Cancer Res* **66**, 7466-7472
10. Singhal, S., Vachani, A., Antin-Ozerkis, D., Kaiser, L. R., and Albelda, S. M. (2005) Prognostic implications of cell cycle, apoptosis, and angiogenesis biomarkers in non-small cell lung cancer: a review. *Clin Cancer Res* **11**, 3974-3986
11. Goffin, J., Lacchetti, C., Ellis, P. M., Ung, Y. C., Evans, W. K., and Lung Cancer Disease Site Group of Cancer Care Ontario's Program in Evidence-Based, C. (2010) First-line systemic chemotherapy in the treatment of advanced non-small cell lung cancer: a systematic review. *J Thorac Oncol* **5**, 260-274
12. Doseff, A. I. (2004) Apoptosis: the sculptor of development. *Stem Cells Dev* **13**, 473-483
13. Horvitz, H. R. (1999) Genetic control of programmed cell death in the nematode Caenorhabditis elegans. *Cancer Res* **59**, 1701s-1706s
14. Degterev, A., Boyce, M., and Yuan, J. (2003) A decade of caspases. *Oncogene* **22**, 8543-8567
15. Miki, K., and Eddy, E. M. (2002) Tumor necrosis factor receptor 1 is an ATPase regulated by silencer of death domain. *Mol Cell Biol* **22**, 2536-2543
16. Jiang, Y., Woronicz, J. D., Liu, W., and Goeddel, D. V. (1999) Prevention of constitutive TNF receptor 1 signaling by silencer of death domains. *Science* **283**, 543-546
17. Chinnaiyan, A. M., O'Rourke, K., Tewari, M., and Dixit, V. M. (1995) FADD, a novel death domain-containing protein, interacts with the death domain of Fas and initiates apoptosis. *Cell* **81**, 505-512
18. Peter, M. E., and Krammer, P. H. (1998) Mechanisms of CD95 (APO-1/Fas)-mediated apoptosis. *Curr Opin Immunol* **10**, 545-551

19. Rosato, R. R., Almenara, J. A., Dai, Y., and Grant, S. (2003) Simultaneous activation of the intrinsic and extrinsic pathways by histone deacetylase (HDAC) inhibitors and tumor necrosis factor-related apoptosis-inducing ligand (TRAIL) synergistically induces mitochondrial damage and apoptosis in human leukemia cells. *Mol Cancer Ther* **2**, 1273-1284
20. Acehan, D., Jiang, X., Morgan, D. G., Heuser, J. E., Wang, X., and Akey, C. W. (2002) Three-dimensional structure of the apoptosome: implications for assembly, procaspase-9 binding, and activation. *Mol Cell* **9**, 423-432
21. Voss, O. H., Batra, S., Kolattukudy, S. J., Gonzalez-Mejia, M. E., Smith, J. B., and Doseff, A. I. (2007) Binding of caspase-3 prodomain to heat shock protein 27 regulates monocyte apoptosis by inhibiting caspase-3 proteolytic activation. *J Biol Chem* **282**, 25088-25099
22. Clementi, M. E., Giardina, B., Di Stasio, E., Mordente, A., and Misiti, F. (2003) Doxorubicin-derived metabolites induce release of cytochrome C and inhibition of respiration on cardiac isolated mitochondria. *Anticancer Res* **23**, 2445-2450
23. Gonzalez-Mejia, M. E., and Doseff, A. I. (2009) Regulation of monocytes and macrophages cell fate. *Front Biosci* **14**, 2413-2431
24. Shi, Y. (2002) Mechanisms of caspase activation and inhibition during apoptosis. *Mol Cell* **9**, 459-470
25. Li, H., Zhu, H., Xu, C. J., and Yuan, J. (1998) Cleavage of BID by caspase 8 mediates the mitochondrial damage in the Fas pathway of apoptosis. *Cell* **94**, 491-501
26. Luo, X., Budihardjo, I., Zou, H., Slaughter, C., and Wang, X. (1998) Bid, a Bcl2 interacting protein, mediates cytochrome c release from mitochondria in response to activation of cell surface death receptors. *Cell* **94**, 481-490
27. Adams, J. M., and Cory, S. (1998) The Bcl-2 protein family: arbiters of cell survival. *Science* **281**, 1322-1326
28. Vander Heiden, M. G., Chandel, N. S., Williamson, E. K., Schumacker, P. T., and Thompson, C. B. (1997) Bcl-xL regulates the membrane potential and volume homeostasis of mitochondria. *Cell* **91**, 627-637
29. Korsmeyer, S. J., Wei, M. C., Saito, M., Weiler, S., Oh, K. J., and Schlesinger, P. H. (2000) Pro-apoptotic cascade activates BID, which oligomerizes BAK or BAX into pores that result in the release of cytochrome c. *Cell Death Differ* **7**, 1166-1173
30. Kuwana, T., Mackey, M. R., Perkins, G., Ellisman, M. H., Latterich, M., Schneiter, R., Green, D. R., and Newmeyer, D. D. (2002) Bid, Bax, and lipids cooperate to form supramolecular openings in the outer mitochondrial membrane. *Cell* **111**, 331-342
31. Deveraux, Q. L., and Reed, J. C. (1999) IAP family proteins--suppressors of apoptosis. *Genes Dev* **13**, 239-252
32. Clem, R. J., and Duckett, C. S. (1997) The IAP genes: unique arbitrators of cell death. *Trends Cell Biol* **7**, 337-339
33. Wang, C. Y., Mayo, M. W., Korneluk, R. G., Goeddel, D. V., and Baldwin, A. S., Jr. (1998) NF-kappaB antiapoptosis: induction of TRAF1 and TRAF2 and c-IAP1 and c-IAP2 to suppress caspase-8 activation. *Science* **281**, 1680-1683
34. Bratton, S. B., Walker, G., Srinivasula, S. M., Sun, X. M., Butterworth, M., Alnemri, E. S., and Cohen, G. M. (2001) Recruitment, activation and retention of caspases-9 and -3 by Apaf-1 apoptosome and associated XIAP complexes. *EMBO J* **20**, 998-1009

35. Fong, W. G., Liston, P., Rajcan-Separovic, E., St Jean, M., Craig, C., and Korneluk, R. G. (2000) Expression and genetic analysis of XIAP-associated factor 1 (XAF1) in cancer cell lines. *Genomics* **70**, 113-122
36. Li, M., Song, T., Yin, Z. F., and Na, Y. Q. (2007) XIAP as a prognostic marker of early recurrence of nonmuscular invasive bladder cancer. *Chin Med J (Engl)* **120**, 469-473
37. Moussata, D., Amara, S., Siddeek, B., Decaussin, M., Hehlgans, S., Paul-Bellon, R., Mornex, F., Gerard, J. P., Romestaing, P., Rodel, F., Flourie, B., Benahmed, M., and Mauduit, C. (2012) XIAP as a radioresistance factor and prognostic marker for radiotherapy in human rectal adenocarcinoma. *Am J Pathol* **181**, 1271-1278
38. Ramp, U., Krieg, T., Caliskan, E., Mahotka, C., Ebert, T., Willers, R., Gabbert, H. E., and Gerharz, C. D. (2004) XIAP expression is an independent prognostic marker in clear-cell renal carcinomas. *Hum Pathol* **35**, 1022-1028
39. Craig, E. A., Gambill, B. D., and Nelson, R. J. (1993) Heat shock proteins: molecular chaperones of protein biogenesis. *Microbiol Rev* **57**, 402-414
40. Sun, Y., and MacRae, T. H. (2005) Small heat shock proteins: molecular structure and chaperone function. *Cell Mol Life Sci* **62**, 2460-2476
41. Augusteyn, R. C. (2004) alpha-crystallin: a review of its structure and function. *Clin Exp Optom* **87**, 356-366
42. Arrigo, A. P., Simon, S., Gibert, B., Kretz-Remy, C., Nivon, M., Czekalla, A., Guillet, D., Moulin, M., Diaz-Latoud, C., and Vicart, P. (2007) Hsp27 (HspB1) and alphaB-crystallin (HspB5) as therapeutic targets. *FEBS Lett* **581**, 3665-3674
43. Gonzalez-Mejia, M. E., Voss, O. H., Murnan, E. J., and Doseff, A. I. (2010) Apigenin-induced apoptosis of leukemia cells is mediated by a bimodal and differentially regulated residue-specific phosphorylation of heat-shock protein-27. *Cell Death Dis* **1**, e64
44. Kostenko, S., and Moens, U. (2009) Heat shock protein 27 phosphorylation: kinases, phosphatases, functions and pathology. *Cell Mol Life Sci* **66**, 3289-3307
45. Zhang, D., Wong, L. L., and Koay, E. S. (2007) Phosphorylation of Ser78 of Hsp27 correlated with HER-2/neu status and lymph node positivity in breast cancer. *Mol Cancer* **6**, 52
46. Bruey, J. M., Ducasse, C., Bonniaud, P., Ravagnan, L., Susin, S. A., Diaz-Latoud, C., Gurbuxani, S., Arrigo, A. P., Kroemer, G., Solary, E., and Garrido, C. (2000) Hsp27 negatively regulates cell death by interacting with cytochrome c. *Nat Cell Biol* **2**, 645-652
47. Kris-Etherton, P. M., Hecker, K. D., Bonanome, A., Coval, S. M., Binkoski, A. E., Hilpert, K. F., Griel, A. E., and Etherton, T. D. (2002) Bioactive compounds in foods: their role in the prevention of cardiovascular disease and cancer. *Am J Med* **113 Suppl 9B**, 71S-88S
48. Narayana, K. R., Reddy, M. S., Chaluvadi, M. R., and Krishna, D. R. (2001) Bioflavonoids classification, pharmacological, biochemical effects and therapeutic potential. *Indian Journal of Pharmacology* **33**, 2-16
49. Cassidy, A., Rimm, E. B., O'Reilly, E. J., Logroscino, G., Kay, C., Chiuve, S. E., and Rexrode, K. M. (2012) Dietary flavonoids and risk of stroke in women. *Stroke* **43**, 946-951

50. Gao, X., Cassidy, A., Schwarzschild, M. A., Rimm, E. B., and Ascherio, A. (2012) Habitual intake of dietary flavonoids and risk of Parkinson disease. *Neurology* **78**, 1138-1145
51. van Dam, R. M., Naidoo, N., and Landberg, R. (2013) Dietary flavonoids and the development of type 2 diabetes and cardiovascular diseases: review of recent findings. *Curr Opin Lipidol* **24**, 25-33
52. Christensen, K. Y., Naidu, A., Parent, M. E., Pintos, J., Abrahamowicz, M., Siemiatycki, J., and Koushik, A. (2012) The risk of lung cancer related to dietary intake of flavonoids. *Nutr Cancer* **64**, 964-974
53. Birt, D. F., Hendrich, S., and Wang, W. (2001) Dietary agents in cancer prevention: flavonoids and isoflavonoids. *Pharmacol Ther* **90**, 157-177
54. Kyle, J. A., Sharp, L., Little, J., Duthie, G. G., and McNeill, G. (2010) Dietary flavonoid intake and colorectal cancer: a case-control study. *Br J Nutr* **103**, 429-436
55. Rossi, M., Bosetti, C., Negri, E., Lagiou, P., and La Vecchia, C. (2010) Flavonoids, proanthocyanidins, and cancer risk: a network of case-control studies from Italy. *Nutr Cancer* **62**, 871-877
56. Manach, C., Scalbert, A., Morand, C., Remesy, C., and Jimenez, L. (2004) Polyphenols: food sources and bioavailability. *Am J Clin Nutr* **79**, 727-747
57. McKay, D. L., and Blumberg, J. B. (2006) A review of the bioactivity and potential health benefits of chamomile tea (Matricaria recutita L.). *Phytother Res* **20**, 519-530
58. Meyer, H., Bolarinwa, A., Wolfram, G., and Linseisen, J. (2006) Bioavailability of apigenin from apiin-rich parsley in humans. *Ann Nutr Metab* **50**, 167-172
59. Patel, D., Shukla, S., and Gupta, S. (2007) Apigenin and cancer chemoprevention: progress, potential and promise (review). *Int J Oncol* **30**, 233-245
60. Middleton, E., Jr., Kandaswami, C., and Theoharides, T. C. (2000) The effects of plant flavonoids on mammalian cells: implications for inflammation, heart disease, and cancer. *Pharmacol Rev* **52**, 673-751
61. Vargo, M. A., Voss, O. H., Poustka, F., Cardounel, A. J., Grotewold, E., and Doseff, A. I. (2006) Apigenin-induced-apoptosis is mediated by the activation of PKCdelta and caspases in leukemia cells. *Biochem Pharmacol* **72**, 681-692
62. Arango, D., Parihar, A., Villamena, F. A., Wang, L., Freitas, M. A., Grotewold, E., and Doseff, A. I. (2012) Apigenin induces DNA damage through the PKCdelta-dependent activation of ATM and H2AX causing down-regulation of genes involved in cell cycle control and DNA repair. *Biochem Pharmacol* **84**, 1571-1580
63. Way, T. D., Kao, M. C., and Lin, J. K. (2004) Apigenin induces apoptosis through proteasomal degradation of HER2/neu in HER2/neu-overexpressing breast cancer cells via the phosphatidylinositol 3-kinase/Akt-dependent pathway. *J Biol Chem* **279**, 4479-4489
64. Knowles, L. M., Zigrossi, D. A., Tauber, R. A., Hightower, C., and Milner, J. A. (2000) Flavonoids suppress androgen-independent human prostate tumor proliferation. *Nutr Cancer* **38**, 116-122
65. Czyz, J., Madeja, Z., Irmer, U., Korohoda, W., and Hulser, D. F. (2005) Flavonoid apigenin inhibits motility and invasiveness of carcinoma cells in vitro. *Int J Cancer* **114**, 12-18

66. Engelmann, C., Blot, E., Panis, Y., Bauer, S., Trochon, V., Nagy, H. J., Lu, H., and Soria, C. (2002) Apigenin--strong cytostatic and anti-angiogenic action in vitro contrasted by lack of efficacy in vivo. *Phytomedicine* **9**, 489-495
67. Farah, M., Parhar, K., Moussavi, M., Eivemark, S., and Salh, B. (2003) 5,6-Dichloro-ribifuranosylbenzimidazole- and apigenin-induced sensitization of colon cancer cells to TNF-alpha-mediated apoptosis. *Am J Physiol Gastrointest Liver Physiol* **285**, G919-928
68. Lindenmeyer, F., Li, H., Menashi, S., Soria, C., and Lu, H. (2001) Apigenin acts on the tumor cell invasion process and regulates protease production. *Nutr Cancer* **39**, 139-147
69. Brusselmans, K., Vrolix, R., Verhoeven, G., and Swinnen, J. V. (2005) Induction of cancer cell apoptosis by flavonoids is associated with their ability to inhibit fatty acid synthase activity. *J Biol Chem* **280**, 5636-5645
70. Kim, M. H. (2003) Flavonoids inhibit VEGF/bFGF-induced angiogenesis in vitro by inhibiting the matrix-degrading proteases. *J Cell Biochem* **89**, 529-538
71. Menichincheri, M., Ballinari, D., Bargiotti, A., Bonomini, L., Ceccarelli, W., D'Alessio, R., Fretta, A., Moll, J., Polucci, P., Soncini, C., Tibolla, M., Trosset, J. Y., and Vanotti, E. (2004) Catecholic flavonoids acting as telomerase inhibitors. *J Med Chem* **47**, 6466-6475
72. Reiners, J. J., Jr., Clift, R., and Mathieu, P. (1999) Suppression of cell cycle progression by flavonoids: dependence on the aryl hydrocarbon receptor. *Carcinogenesis* **20**, 1561-1566
73. Budihardjo, I., Oliver, H., Lutter, M., Luo, X., and Wang, X. (1999) Biochemical pathways of caspase activation during apoptosis. *Annu Rev Cell Dev Biol* **15**, 269-290
74. Hakem, R., Hakem, A., Duncan, G. S., Henderson, J. T., Woo, M., Soengas, M. S., Elia, A., de la Pompa, J. L., Kagi, D., Khoo, W., Potter, J., Yoshida, R., Kaufman, S. A., Lowe, S. W., Penninger, J. M., and Mak, T. W. (1998) Differential requirement for caspase 9 in apoptotic pathways in vivo. *Cell* **94**, 339-352
75. Sun, X. M., MacFarlane, M., Zhuang, J., Wolf, B. B., Green, D. R., and Cohen, G. M. (1999) Distinct caspase cascades are initiated in receptor-mediated and chemical-induced apoptosis. *J Biol Chem* **274**, 5053-5060
76. Minotti, G., Menna, P., Salvatorelli, E., Cairo, G., and Gianni, L. (2004) Anthracyclines: molecular advances and pharmacologic developments in antitumor activity and cardiotoxicity. *Pharmacol Rev* **56**, 185-229
77. Giaccone, G., Linn, S. C., Welink, J., Catimel, G., Stieltjes, H., van der Vijgh, W. J., Eeltink, C., Vermorken, J. B., and Pinedo, H. M. (1997) A dose-finding and pharmacokinetic study of reversal of multidrug resistance with SDZ PSC 833 in combination with doxorubicin in patients with solid tumors. *Clin Cancer Res* **3**, 2005-2015
78. Hequet, O., Le, Q. H., Moullet, I., Pauli, E., Salles, G., Espinouse, D., Dumontet, C., Thieblemont, C., Arnaud, P., Antal, D., Bouafia, F., and Coiffier, B. (2004) Subclinical late cardiomyopathy after doxorubicin therapy for lymphoma in adults. *J Clin Oncol* **22**, 1864-1871
79. Wilson, R. E., Wood, W. C., Lerner, H. L., Antman, K., Amato, D., Corson, J. M., Proppe, K., Harmon, D., Carey, R., Greenberger, J., and et al. (1986) Doxorubicin

chemotherapy in the treatment of soft-tissue sarcoma. Combined results of two randomized trials. *Arch Surg* **121**, 1354-1359
80. Zambetti, M., Moliterni, A., Materazzo, C., Stefanelli, M., Cipriani, S., Valagussa, P., Bonadonna, G., and Gianni, L. (2001) Long-term cardiac sequelae in operable breast cancer patients given adjuvant chemotherapy with or without doxorubicin and breast irradiation. *J Clin Oncol* **19**, 37-43
81. Zheng, J. H., Chen, C. T., Au, J. L., and Wientjes, M. G. (2001) Time- and concentration-dependent penetration of doxorubicin in prostate tumors. *AAPS PharmSci* **3**, E15
82. Turakhia, S., Venkatakrishnan, C. D., Dunsmore, K., Wong, H., Kuppusamy, P., Zweier, J. L., and Ilangovan, G. (2007) Doxorubicin-induced cardiotoxicity: direct correlation of cardiac fibroblast and H9c2 cell survival and aconitase activity with heat shock protein 27. *Am J Physiol Heart Circ Physiol* **293**, H3111-3121
83. Zhuang, H., Jiang, W., Cheng, W., Qian, K., Dong, W., Cao, L., Huang, Q., Li, S., Dou, F., Chiu, J. F., Fang, X. X., Lu, M., and Hua, Z. C. (2010) Down-regulation of HSP27 sensitizes TRAIL-resistant tumor cell to TRAIL-induced apoptosis. *Lung Cancer* **68**, 27-38
84. Garrido, C., Brunet, M., Didelot, C., Zermati, Y., Schmitt, E., and Kroemer, G. (2006) Heat shock proteins 27 and 70: anti-apoptotic proteins with tumorigenic properties. *Cell Cycle* **5**, 2592-2601
85. Venkatakrishnan, C. D., Dunsmore, K., Wong, H., Roy, S., Sen, C. K., Wani, A., Zweier, J. L., and Ilangovan, G. (2008) HSP27 regulates p53 transcriptional activity in doxorubicin-treated fibroblasts and cardiac H9c2 cells: p21 upregulation and G2/M phase cell cycle arrest. *Am J Physiol Heart Circ Physiol* **294**, H1736-1744
86. Liu, L., Zhang, X., Qian, B., Min, X., Gao, X., Li, C., Cheng, Y., and Huang, J. (2007) Over-expression of heat shock protein 27 attenuates doxorubicin-induced cardiac dysfunction in mice. *Eur J Heart Fail* **9**, 762-769
87. Venkatakrishnan, C. D., Tewari, A. K., Moldovan, L., Cardounel, A. J., Zweier, J. L., Kuppusamy, P., and Ilangovan, G. (2006) Heat shock protects cardiac cells from doxorubicin-induced toxicity by activating p38 MAPK and phosphorylation of small heat shock protein 27. *Am J Physiol Heart Circ Physiol* **291**, H2680-2691
88. Gerrelli, D., Grimaldi, K., Horn, D., Mahadeva, U., Sharpe, N., and Latchman, D. S. (1993) The cardiac form of the tissue-specific SmN protein is identical to the brain and embryonic forms of the protein. *J Mol Cell Cardiol* **25**, 321-329
89. Hescheler, J., Meyer, R., Plant, S., Krautwurst, D., Rosenthal, W., and Schultz, G. (1991) Morphological, biochemical, and electrophysiological characterization of a clonal cell (H9c2) line from rat heart. *Circ Res* **69**, 1476-1486
90. Hsu, H. S., Lin, J. H., Huang, W. C., Hsu, T. W., Su, K., Chiou, S. H., Tsai, Y. T., and Hung, S. C. (2011) Chemoresistance of lung cancer stemlike cells depends on activation of Hsp27. *Cancer* **117**, 1516-1528
91. Kim, K. K., Kim, R., and Kim, S. H. (1998) Crystal structure of a small heat-shock protein. *Nature* **394**, 595-599
92. van Montfort, R. L., Basha, E., Friedrich, K. L., Slingsby, C., and Vierling, E. (2001) Crystal structure and assembly of a eukaryotic small heat shock protein. *Nat Struct Biol* **8**, 1025-1030

93. Hilario, E., Martin, F. J., Bertolini, M. C., and Fan, L. (2011) Crystal structures of Xanthomonas small heat shock protein provide a structural basis for an active molecular chaperone oligomer. *J Mol Biol* **408**, 74-86
94. Stamler, R., Kappe, G., Boelens, W., and Slingsby, C. (2005) Wrapping the alpha-crystallin domain fold in a chaperone assembly. *J Mol Biol* **353**, 68-79
95. Baranova, E. V., Beelen, S., Gusev, N. B., and Strelkov, S. V. (2009) The taming of small heat-shock proteins: crystallization of the alpha-crystallin domain from human Hsp27. *Acta Crystallogr Sect F Struct Biol Cryst Commun* **65**, 1277-1281
96. Baranova, E. V., Weeks, S. D., Beelen, S., Bukach, O. V., Gusev, N. B., and Strelkov, S. V. (2011) Three-dimensional structure of alpha-crystallin domain dimers of human small heat shock proteins HSPB1 and HSPB6. *J Mol Biol* **411**, 110-122
97. Kelley, S. K., Harris, L. A., Xie, D., Deforge, L., Totpal, K., Bussiere, J., and Fox, J. A. (2001) Preclinical studies to predict the disposition of Apo2L/tumor necrosis factor-related apoptosis-inducing ligand in humans: characterization of in vivo efficacy, pharmacokinetics, and safety. *J Pharmacol Exp Ther* **299**, 31-38
98. Ashkenazi, A., Pai, R. C., Fong, S., Leung, S., Lawrence, D. A., Marsters, S. A., Blackie, C., Chang, L., McMurtrey, A. E., Hebert, A., DeForge, L., Koumenis, I. L., Lewis, D., Harris, L., Bussiere, J., Koeppen, H., Shahrokh, Z., and Schwall, R. H. (1999) Safety and antitumor activity of recombinant soluble Apo2 ligand. *J Clin Invest* **104**, 155-162
99. Walczak, H., Miller, R. E., Ariail, K., Gliniak, B., Griffith, T. S., Kubin, M., Chin, W., Jones, J., Woodward, A., Le, T., Smith, C., Smolak, P., Goodwin, R. G., Rauch, C. T., Schuh, J. C., and Lynch, D. H. (1999) Tumoricidal activity of tumor necrosis factor-related apoptosis-inducing ligand in vivo. *Nat Med* **5**, 157-163
100. Daniel, P. T., Wieder, T., Sturm, I., and Schulze-Osthoff, K. (2001) The kiss of death: promises and failures of death receptors and ligands in cancer therapy. *Leukemia* **15**, 1022-1032
101. Guo, F., Sigua, C., Bali, P., George, P., Fiskus, W., Scuto, A., Annavarapu, S., Mouttaki, A., Sondarva, G., Wei, S., Wu, J., Djeu, J., and Bhalla, K. (2005) Mechanistic role of heat shock protein 70 in Bcr-Abl-mediated resistance to apoptosis in human acute leukemia cells. *Blood* **105**, 1246-1255
102. Hoogwater, F. J., Nijkamp, M. W., Smakman, N., Steller, E. J., Emmink, B. L., Westendorp, B. F., Raats, D. A., Sprick, M. R., Schaefer, U., Van Houdt, W. J., De Bruijn, M. T., Schackmann, R. C., Derksen, P. W., Medema, J. P., Walczak, H., Borel Rinkes, I. H., and Kranenburg, O. (2010) Oncogenic K-Ras turns death receptors into metastasis-promoting receptors in human and mouse colorectal cancer cells. *Gastroenterology* **138**, 2357-2367
103. Trauzold, A., Siegmund, D., Schniewind, B., Sipos, B., Egberts, J., Zorenkov, D., Emme, D., Roder, C., Kalthoff, H., and Wajant, H. (2006) TRAIL promotes metastasis of human pancreatic ductal adenocarcinoma. *Oncogene* **25**, 7434-7439
104. Stegehuis, J. H., de Wilt, L. H., de Vries, E. G., Groen, H. J., de Jong, S., and Kruyt, F. A. (2010) TRAIL receptor targeting therapies for non-small cell lung cancer: current status and perspectives. *Drug Resist Updat* **13**, 2-15
105. Kuhar, M., Sen, S., and Singh, N. (2006) Role of mitochondria in quercetin-enhanced chemotherapeutic response in human non-small cell lung carcinoma H-520 cells. *Anticancer Res* **26**, 1297-1303

106. Li, Y., Ahmed, F., Ali, S., Philip, P. A., Kucuk, O., and Sarkar, F. H. (2005) Inactivation of nuclear factor kappaB by soy isoflavone genistein contributes to increased apoptosis induced by chemotherapeutic agents in human cancer cells. *Cancer Res* **65**, 6934-6942
107. Tang, X., Wang, H., Fan, L., Wu, X., Xin, A., Ren, H., and Wang, X. J. (2011) Luteolin inhibits Nrf2 leading to negative regulation of the Nrf2/ARE pathway and sensitization of human lung carcinoma A549 cells to therapeutic drugs. *Free Radic Biol Med* **50**, 1599-1609
108. Cai, X., Ye, T., Liu, C., Lu, W., Lu, M., Zhang, J., Wang, M., and Cao, P. (2011) Luteolin induced G2 phase cell cycle arrest and apoptosis on non-small cell lung cancer cells. *Toxicol In Vitro* **25**, 1385-1391
109. Szliszka, E., Czuba, Z. P., Jernas, K., and Krol, W. (2008) Dietary flavonoids sensitize HeLa cells to tumor necrosis factor-related apoptosis-inducing ligand (TRAIL). *Int J Mol Sci* **9**, 56-64
110. Sherman, M., and Multhoff, G. (2007) Heat shock proteins in cancer. *Ann N Y Acad Sci* **1113**, 192-201
111. Jakubowicz-Gil, J., Rzymowska, J., and Gawron, A. (2002) Quercetin, apoptosis, heat shock. *Biochem Pharmacol* **64**, 1591-1595
112. Lee, H. Z., Yang, W. H., Bao, B. Y., and Lo, P. L. (2010) Proteomic analysis reveals ATP-dependent steps and chaperones involvement in luteolin-induced lung cancer CH27 cell apoptosis. *Eur J Pharmacol* **642**, 19-27
113. Rusak, G., Gutzeit, H. O., and Ludwig-Muller, J. (2002) Effects of structurally related flavonoids on Hsp gene expression in human promyeloid leukaemia cells. *Food Technol. Biotechnol.* **40**, 267-273
114. Shi, R. X., Ong, C. N., and Shen, H. M. (2005) Protein kinase C inhibition and x-linked inhibitor of apoptosis protein degradation contribute to the sensitization effect of luteolin on tumor necrosis factor-related apoptosis-inducing ligand-induced apoptosis in cancer cells. *Cancer Res* **65**, 7815-7823
115. Kelley, R. F., Totpal, K., Lindstrom, S. H., Mathieu, M., Billeci, K., Deforge, L., Pai, R., Hymowitz, S. G., and Ashkenazi, A. (2005) Receptor-selective mutants of apoptosis-inducing ligand 2/tumor necrosis factor-related apoptosis-inducing ligand reveal a greater contribution of death receptor (DR) 5 than DR4 to apoptosis signaling. *J Biol Chem* **280**, 2205-2212
116. Chen, W., Wang, X., Zhuang, J., Zhang, L., and Lin, Y. (2007) Induction of death receptor 5 and suppression of survivin contribute to sensitization of TRAIL-induced cytotoxicity by quercetin in non-small cell lung cancer cells. *Carcinogenesis* **28**, 2114-2121
117. Horinaka, M., Yoshida, T., Shiraishi, T., Nakata, S., Wakada, M., and Sakai, T. (2006) The dietary flavonoid apigenin sensitizes malignant tumor cells to tumor necrosis factor-related apoptosis-inducing ligand. *Mol Cancer Ther* **5**, 945-951
118. Jin, C. Y., Park, C., Hwang, H. J., Kim, G. Y., Choi, B. T., Kim, W. J., and Choi, Y. H. (2011) Naringenin up-regulates the expression of death receptor 5 and enhances TRAIL-induced apoptosis in human lung cancer A549 cells. *Mol Nutr Food Res* **55**, 300-309
119. Zhuang, H., Jiang, W., Zhang, X., Qiu, F., Gan, Z., Cheng, W., Zhang, J., Guan, S., Tang, B., Huang, Q., Wu, X., Huang, X., Jiang, W., Hu, Q., Lu, M., and Hua, Z. C. (2013) Suppression of HSP70 expression sensitizes NSCLC cell lines to TRAIL-induced

apoptosis by upregulating DR4 and DR5 and downregulating c-FLIP-L expressions. *J Mol Med (Berl)* **91**, 219-235
120. Pandey, P., Farber, R., Nakazawa, A., Kumar, S., Bharti, A., Nalin, C., Weichselbaum, R., Kufe, D., and Kharbanda, S. (2000) Hsp27 functions as a negative regulator of cytochrome c-dependent activation of procaspase-3. *Oncogene* **19**, 1975-1981
121. Zavialov, A., Benndorf, R., Ehrnsperger, M., Zav'yalov, V., Dudich, I., Buchner, J., and Gaestel, M. (1998) The effect of the intersubunit disulfide bond on the structural and functional properties of the small heat shock protein Hsp25. *Int J Biol Macromol* **22**, 163-173
122. Liu, L. Z., Fang, J., Zhou, Q., Hu, X., Shi, X., and Jiang, B. H. (2005) Apigenin inhibits expression of vascular endothelial growth factor and angiogenesis in human lung cancer cells: implication of chemoprevention of lung cancer. *Mol Pharmacol* **68**, 635-643
123. Lu, H. F., Chie, Y. J., Yang, M. S., Lee, C. S., Fu, J. J., Yang, J. S., Tan, T. W., Wu, S. H., Ma, Y. S., Ip, S. W., and Chung, J. G. (2010) Apigenin induces caspase-dependent apoptosis in human lung cancer A549 cells through Bax- and Bcl-2-triggered mitochondrial pathway. *Int J Oncol* **36**, 1477-1484
124. Gupta, S., Afaq, F., and Mukhtar, H. (2002) Involvement of nuclear factor-kappa B, Bax and Bcl-2 in induction of cell cycle arrest and apoptosis by apigenin in human prostate carcinoma cells. *Oncogene* **21**, 3727-3738
125. Wang, I. K., Lin-Shiau, S. Y., and Lin, J. K. (1999) Induction of apoptosis by apigenin and related flavonoids through cytochrome c release and activation of caspase-9 and caspase-3 in leukaemia HL-60 cells. *Eur J Cancer* **35**, 1517-1525
126. Zheng, P. W., Chiang, L. C., and Lin, C. C. (2005) Apigenin induced apoptosis through p53-dependent pathway in human cervical carcinoma cells. *Life Sci* **76**, 1367-1379
127. Zhang, L., and Fang, B. (2005) Mechanisms of resistance to TRAIL-induced apoptosis in cancer. *Cancer Gene Ther* **12**, 228-237
128. Garofalo, M., Quintavalle, C., Di Leva, G., Zanca, C., Romano, G., Taccioli, C., Liu, C. G., Croce, C. M., and Condorelli, G. (2008) MicroRNA signatures of TRAIL resistance in human non-small cell lung cancer. *Oncogene* **27**, 3845-3855
129. Ding, J., Polier, G., Kohler, R., Giaisi, M., Krammer, P. H., and Li-Weber, M. (2012) Wogonin and related natural flavones overcome tumor necrosis factor-related apoptosis-inducing ligand (TRAIL) protein resistance of tumors by down-regulation of c-FLIP protein and up-regulation of TRAIL receptor 2 expression. *J Biol Chem* **287**, 641-649